

Development of a Multi-disciplinary Design Optimization Framework for a Strut-Braced
Wing Transport Aircraft in PACELAB APD 3.1

Benjamin Kirby Riggins

Thesis submitted to the faculty of the Virginia Polytechnic Institute and State University
in partial fulfillment of the requirements for the degree of

Master of Science
In
Aerospace Engineering

Joseph A. Schetz, Chair
Rakesh K. Kapania, Co-Chair
Davide Locatelli
Pradeep Raj

2/23/2015
Blacksburg, VA

Development of a Multi-disciplinary Design Optimization Framework for a Strut-Braced Wing Transport Aircraft in PACELAB APD 3.1

Benjamin Kirby Riggins

ABSTRACT

The purpose of this study was to extend the analysis methods in PACELAB APD 3.1, a recent commercially available aircraft preliminary design tool with potential for MDO applications, for higher fidelity with physics-based instead of empirical methods and to enable the analysis of nonconventional aircraft configurations. The implementation of these methods was first validated against both existing models and wind tunnel data. Then, the original and extended PACELAB APD versions were used to perform minimum-fuel optimizations for both a traditional cantilever and strut-braced wing aircraft for a medium-range regional transport mission similar to that of a 737-type aircraft, with a minimum range of 3,115 nm and a cruise Mach number of 0.78. The aerodynamics, engine size / weight estimation and structural modules were heavily modified and extended to accomplish this. Comparisons to results for the same mission generated with FLOPS and VT MDO are also discussed.

For the strut-braced configuration, large fuel savings on the order of 37% over the baseline 737-800 aircraft are predicted, while for the cantilever aircraft savings of 10-30% are predicted depending on whether the default or VT methods are utilized in the PACELAB analysis. This demonstrates the potential of the strut-braced configuration for reducing fuel costs, as well as the benefit of MDO in the aircraft conceptual design process. For the cantilever aircraft, FLOPS and VT MDO predict fuel savings of 8% and 23%, respectively. VT MDO predicts a fuel savings of 28% for the strut-braced aircraft over the baseline.

ACKNOWLEDGEMENTS

Without the support from Safran SNECMA this project would not have been possible. Thanks to Thomas Poquet, Bernard Robic and Clement Leenaert for their support, guidance and collaboration over the last two years in a landmark effort representing the first time SNECMA has collaborated directly with Virginia Tech.

The guidance and encouragement provided by my advisors here at Virginia Tech, Dr. Joseph Schetz and Dr. Rakesh Kapania, and research faculty member Dr. Davide Locatelli, has been invaluable in my professional growth. Thanks to Dr. Locatelli for his work on the structural module in PACELAB APD, as well as his superb direction and leadership for the duration of the project. Thanks to Mathias Emeneth of PACE GmbH, and Mark Guynn of NASA LaRC, for their excellent technical support as well.

Special thanks goes to my colleagues and fellow graduate students, in the AOE department and elsewhere, for their support and friendship the last couple years, including but not limited to Nathan Love, Dan Cadel, Brady Doepke, Tobias Ecker, John Gilbert, Wrik Mallik, Tyler Englerth, David Wisda, and Alex Schneider. Thanks to the graduate community in general within the department for providing a positive, productive and engaging environment.

And finally, a very, very special thanks to my family, whose support and encouragement during my time in graduate school could not have been surpassed. Thanks to my parents, David and Patricia Riggins, for instilling in me a love of knowledge and the confidence to pursue it, and to my sister Laura Riggins for her unfailing love and support.

Table of Contents

CHAPTER 1: Introduction	1
1.1 Aircraft Optimization Problem Description.....	1
1.2 Choice of Objective Function	3
1.3 Overview of Main Features of PACELAB, VT MDO and FLOPS.....	6
1.3.1 PACELAB APD 3.1	6
1.3.2 VT MDO.....	8
1.3.3 FLOPS.....	11
1.4 Wing Parameterization and Design Variables	12
1.4.1 Wing Geometric Parameterization.....	13
1.4.2 Design Variables.....	17
1.5 Baseline Aircraft and Mission.....	20
1.6 Optimization Frameworks.....	22
1.6.1 PACELAB APD 3.1 Optimization	22
1.6.2 VT MDO Optimization.....	24
1.6.3 FLOPS Optimization	25
CHAPTER 2: Physics-Based Modifications to PACELAB APD	27
2.1 Aerodynamic Models	27
2.1.1 Induced Drag.....	28
2.1.2 Profile Drag.....	29
2.1.3 Wave Drag	40
2.1.4 Interference Drag	43
2.1.5 Aerodynamic Methods Validation.....	47
2.2 Strut-Braced Wing Cases	70
2.3 Other Models Implemented in PACELAB-VT.....	72
2.3.1 Wing Weight Estimation Model.....	72
2.3.2 Engine Scaling Model.....	77
CHAPTER 3: Aircraft Design Studies	79
3.1 Cantilever Aircraft Designs.....	79
3.2 Strut-Braced Wing Aircraft Designs	83
CHAPTER 4: Conclusions	86
References.....	88

List of Figures

Figure 1. Average carrier fuel costs from 2000 - 2015 ¹³	4
Figure 2. PACELAB APD 3.1 user interface	7
Figure 3. VT MDO Program Flow and Direction ⁵	10
Figure 4. PACELAB APD 3.1 wing parameterization ²¹	14
Figure 5. PACELAB-VT strut parameterization	15
Figure 6. VT MDO planar surface parameterization ²²	16
Figure 7. VT MDO defined cross sections	17
Figure 8. Mission profile and baseline aircraft ¹⁴	21
Figure 9. Transition calculation based on technology factor and leading edge sweep ⁸ ...	33
Figure 10. Differences in planar and body form factors ⁸	39
Figure 11. Wing-fuselage intersection angle ¹⁴	43
Figure 12. PACELAB inclination angle calculation.....	45
Figure 13. DLR-F4 wing body model ⁸	48
Figure 14. Elliptical distribution vs. VT MDO Trefftz plane method, DLR-F4 wing	50
Figure 15. DLR-F4 drag polar predicted with PACELAB-VT (Mach 0.75, Relative Reynolds Number $3.0E6 \text{ ft}^{-1}$).....	51
Figure 16. Pacelab 737-800 model (left) and VT MDO model (right).....	52
Figure 17. 737-800 drag polar (Mach 0.8, Alt 35000 ft)	53
Figure 18. 737-800 drag polar (Mach 0.7, Alt 30000 ft)	54
Figure 19. 737-800 drag polar (Mach 0.6, Alt 25000 ft)	54
Figure 20. Total drag coefficient % difference comparison (737-800)	56
Figure 21. Total drag coefficient drag count difference comparison (737-800).....	56
Figure 22. Elliptical and calculated efficiency comparison (Mach 0.2, 747-800).....	58
Figure 23. Profile drag coefficient % difference comparison (737-800).....	59
Figure 24. Profile drag coefficient drag count difference comparison (737-800)	60
Figure 25. Interference drag coefficient % difference comparison (737-800)	61
Figure 26. Interference drag coefficient drag count difference comparison (737-800)....	61
Figure 27. Wave drag coefficient % difference comparison (737-800)	62
Figure 28. Wave drag coefficient drag count difference comparison (737-800).....	63
Figure 29. 737-800 wing lift distribution comparison between Trefftz plane and elliptical	64
Figure 30. 737-800 wing section lift coefficient comparison between Trefftz plane and elliptical.....	65
Figure 31. 737-800 relative difference in section Cl across wing (CL = 0.8)	66
Figure 32. 737-800 relative difference in critical Mach across wing (CL = 0.8)	66
Figure 33. 737-800 relative difference in Cdw across wing (CL = 0.8).....	67
Figure 34. Induced drag coefficient % difference comparison (737-800).....	67
Figure 35. Induced drag coefficient drag count difference comparison (737-800)	68
Figure 36. Fuselage relative effects on induced drag coefficient comparison (Mach 0.2, 737-800).....	70
Figure 37. Fuselage absolute effects on induced drag coefficient comparison (Mach 0.2, 737-800).....	70
Figure 38. Wing box model	74
Figure 39. Bending stiffness validation for new PACELAB method ²⁷	75

Figure 40. Shevell's wing weight curve with predictions from VT MDO, PACELAB APD 3.1 (Torenbeek), PACELAB-VT (Locatelli), Raymer and Nicolai. 737-800 on the left, 777 on the right.....	76
Figure 41. Optimized cantilever aircraft in PACELAB APD 3.1 (left) and PACELAB-VT(right).....	80
Figure 42. Optimized cantilever aircraft from FLOPS (left) and VT MDO (right)	82
Figure 43. Wave drag rise for 737-800 model in default PACELAB and FLOPS ⁴⁰	83
Figure 44. PACELAB optimized SBW (left) and VT MDO optimized SBW (right).....	85

List of Tables

Table 1. PACELAB-VT design variables (cantilever in black, SBW in red).....	18
Table 2. VT MDO design variables (cantilever in black, SBW in red).....	18
Table 3. FLOPS design variables (cantilever only).....	19
Table 4. Wing geometric constraints	19
Table 5. FLOPS configuration characteristics available for minimization or maximization	25
Table 6. Profile drag user-set parameters	31
Table 7. Laminar skin friction variables	34
Table 8. Laminar skin friction formulas	34
Table 9. Turbulent skin friction variables.....	35
Table 10. Turbulent skin friction formulas	36
Table 11. Form factor variables	37
Table 12. Form factor options and formulas.....	38
Table 13. Wave drag user input parameter	40
Table 14. Wave drag variables.....	42
Table 15. Wave drag formulas.....	42
Table 16. Interference drag user-set parameter.....	44
Table 17. Variables for Hoerner model	46
Table 18. Formulas for Hoerner model.....	46
Table 19. Variables for Tetrault model.....	47
Table 20. Formulas for Tetrault model	47
Table 21. DLRF-4 code comparison results (Mach 0.8, Relative Re $6.54E6 \text{ ft}^{-1}$, Lift Coefficient 0.7). VT MDO code vs. PACELAB-VT.....	49
Table 22. Load cases for wing sizing ³⁸	72
Table 23. Wing weight predictions for both a 737-800 and 777 size aircraft	75
Table 24. Engine reference values ¹⁴	78
Table 25. Optimized minimum fuel cantilever aircraft	81
Table 26. Optimized minimum fuel SBW aircraft.....	84

CHAPTER 1: Introduction

1.1 Aircraft Optimization Problem Description

Issues that need to be addressed in the conceptual aircraft design phase relate to the geometric dimensions and weight of the airplane¹, as well as propulsion and aerodynamic concerns, so as to ensure a feasible concept is being pursued for further detailed design. This necessitates a linking of the various aircraft disciplines, hence the multi-disciplinary nature of aircraft preliminary design². The problem becomes more than a question of a mere single analysis, however, as it is the task of the designer to select the configuration that resembles the ‘best’ airplane for completing the mission and meeting the design requirements, in an iterative process.

This is where the field of multi-disciplinary design optimization (MDO) enters into the design process. While in the past achieving an optimal design was a costly and painstaking process, with the aid of modern computers MDO has been made faster and less costly to accomplish with numerous applications in the aerospace design process³. Given a set of design variables (aircraft and / or mission parameters to be varied during an optimization) and an objective function (TOGW, fuel consumption, lift-to-drag ratio, etc.) to be minimized, nonlinear programming techniques can be used to find local extrema in the design space that translate to an ‘optimal’ design that is dependent on the initial starting values of the design variables; that is, where in the design space the initial aircraft lies⁴. Using global-search techniques such as genetic algorithms the entirety of the design space can be explored and a global minimum can be approached, within a degree of uncertainty. This lessens the dependency of the final solution on the initial

conditions, but results in greater importance on the boundaries of the design space (to prevent infeasible solutions near the boundaries) and, usually, highly increased runtimes on the order of days, not hours. In practice the global-search approach is often used to generate an ‘initial’ set of results with a small number of iterations and then a faster gradient-based optimizer is used to find a minimum in the region of these initial results⁵.

For a conventional aircraft configuration, such as the tube-and-wing type seen in most modern subsonic transport aircraft, empirical or semi-empirical methods can be utilized to simplify the design process, limit the number of design variables and speed the computation⁶. However, this limits the longevity of the software as it does not take into account technological improvements over time⁷. In addition, as the complexity of the airplane increases, such as in a non-conventional aircraft configuration for which empirical data and methods may not exist, the problem of modeling such characteristics as aerodynamics and component weights in the MDO analysis becomes magnified. One possible answer to this problem is a heavier emphasis on physics-based methods for analyzing aircraft performance, which are more ‘general’ in nature than empirical methods and can be applied to more exotic aircraft configurations for which experimental data may not exist⁸. Implementing these types of methods usually entails increasing the number of design variables and the complexity of the computation.

In the course of this study existing empirical methods^{1,6} in PACELAB APD 3.1 were augmented with physics-based methods for aerodynamic calculations, taken from past work and existing MDO software⁵ at Virginia Tech (hereafter referred to as VT MDO). The default methods in PACELAB APD 3.1 are empirical relations developed for conventional tube-and-wing aircraft by Raymer¹ and Torenbeek⁶. For non-conventional

aircraft such as a strut-braced wing (hereafter referred to as SBW) configuration these methods are insufficient for drag calculations, hence the need for more generally applicable methods. In a problem similar to that with the aerodynamics, conventional structural weight methods cannot accurately size the wing due to the presence of a strut, which provides a weight benefit to the wing by reducing bending moment. Therefore, to complete the optimizations presented at the end of this thesis, a new method based on VT MDO and further developed by Dr. Davide Locatelli for calculating wing weight was also utilized. In addition, a simple model taken directly from VT MDO for scaling engine size and weight based on maximum sea level static thrust was implemented⁵.

For clarity and consistency, the default ‘out of the box’ PACELAB software is hereafter referred to as ‘PACELAB APD’, and the modified PACELAB APD updated with the new methods is referred to as ‘PACELAB-VT’. When referring to both software versions, only the term ‘PACELAB’ appears.

1.2 Choice of Objective Function

The first step in any optimization is the definition of the objective function; that is, answering the question of what particular performance characteristic is being optimized. For a transport aircraft this could include performance metrics such as range, endurance (minimum fuel flow), lift-to-drag ratio, minimum fuel mass or minimum TOGW. Other metrics can also be of interest as well, including environmental impact⁹, manufacturing cost¹⁰, and/or some combination of these.

TOGW has a direct relationship to the total life-cycle cost of an aircraft configuration for the aircraft operator, thus making it an attractive parameter for

minimization, and it has been the subject of many MDO studies over the years, at Virginia Tech and elsewhere^{11,12}.

Minimum fuel consumption has become increasingly relevant in the past few decades as fuel costs have risen¹³ and environmental concerns have become increasingly visible in the global consciousness. Figure 1 shows the average monthly cost-per-gallon spent by all large aircraft carriers in the United States over the past fifteen years.

Adjusting for inflation, current prices are about 170% higher than they were in the year 2000. While prices fluctuate quite a bit as can be seen in the figure, the overall trend is upward and as the world's population increases and the world economy becomes increasingly globalized, demand can be expected to increase and fuel costs will likely keep rising in the foreseeable future.



Figure 1. Average carrier fuel costs from 2000 - 2015¹³.

Therefore, designs that can complete a mission with a minimum of total on-board fuel represent both significant savings for airlines in fuel purchases (lower operational costs), as well as a reduction of emissions being dumped into the atmosphere on a per-mission basis. For a SBW type aircraft, which is a more efficient, lower-drag vehicle than a traditional cantilever design, minimum fuel designs are particularly attractive as the SBW configuration provides a direct benefit to fuel consumption for a given mission. This is a consequence of the increased span and lower thickness ratio of the wing, thanks to the structural benefit of the strut's presence, resulting in lower induced drag throughout the mission and better transonic behavior in the cruise flight regime due to the reduction in wave drag. In addition, reduced sweep, chord and thickness ratio permit more natural laminar flow over the wing. For the final part of this study, minimum fuel optimization runs were performed in PACELAB for a baseline cantilever aircraft representative of a subsonic medium-range regional airliner (similar to the B737-800 Next Generation), and the results were compared to those of a past study conducted in VT MDO with a similar aircraft model¹⁴, as well as optimization results for the same mission with the PACELAB default methods and FLOPS². A high-wing SBW aircraft derived from this baseline model was also optimized for minimum fuel for the same mission.

An important difference in the study conducted here for the SBW is the assumption of a non-lifting strut throughout the mission. Because struts are designed for tension / compression and not bending, it is desirable to minimize normal force on the strut during cruise configuration. This, of course, has an impact on the induced drag of the configuration, which will in turn impact the design of the wing and strut structure. The drag due to lift on the strut can be significant; a recent study conducted by NASA

Ames of the Boeing SUGAR TBW model found the induced drag contribution of the struts to be as high as 7% of the overall aircraft drag coefficient¹⁵.

1.3 Overview of Main Features of PACELAB, VT MDO and FLOPS

1.3.1 PACELAB APD 3.1

PACELAB APD 3.1 is an aircraft preliminary design software, developed by the German engineering firm PACE GmbH, with an emphasis on flexibility and user-friendliness. Unlike veteran MDO preliminary design applications such as FLOPS and VT MDO, PACELAB APD 3.1 is built around a graphical user interface (see Figure 2) that gives a 3D representation of the aircraft geometry, as well as a quick view of parameter values in the mathematical model, both input and output. Parameters are grouped in node-like structures (or ‘modules’) that appear in a tree-like diagram in the left hand panes of the user interface. Parameters can also have their input/output status switched, though this requires careful balancing of input / output parameters to prevent an under- or over-constrained mathematical system. Analysis / optimizations are performed in Engineering Work Bench, the ‘front program’ that is meant for end-users. Constraints can be defined on any parameter within the workspace to ensure feasible designs, or define a specific mission.

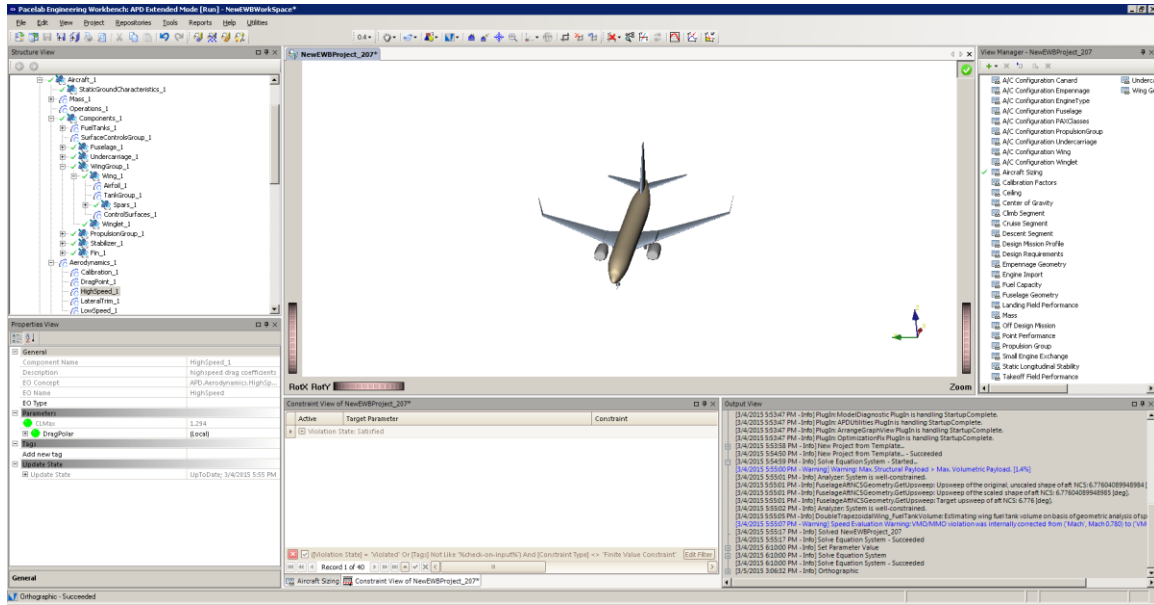


Figure 2. PACELAB APD 3.1 user interface

The features listed above are of great interest to MDO end-users who wish to easily manipulate their data model and quickly visualize their aircraft in physical space. Advanced users who wish to add their own analysis methods, or change existing methods to their liking, can utilize the Knowledge Designer, a backend programming tool similar to Microsoft Visual Studio, to code additional modules in C# or edit existing ones. This capability allows for the APD software to be extended in any conceivable way to handle new or exotic aircraft configurations, which was the focus of this study.

PACELAB APD 3.1 analysis methods are based heavily on empirical methods from Torenbeek⁶ and Raymer¹, as well as a point-by-point mission performance analysis module developed in-house by PACE GmbH³⁶. Other performance metrics available include a simple stability calculation for static margin, and the modules for aerodynamic performance and aircraft weights. The latter two are of particular note, as these are

replaced in PACELAB-VT by physics-based methods based on past work in VT MDO.

PACELAB APD 3.1 analysis methods can be broken down into three categories:

1. Weight estimation. Includes methods for calculating the weights of the airframe components, that is, the wing, fuselage, empennage, landing gear and engine nacelles. Also calculates propulsion and payload weights, as well as accounting for the additional weights of onboard equipment / services and operational items.
2. Aerodynamic performance. Predicts lift coefficients and lift curve slopes of wing and stabilizer surfaces given 2-D airfoil data (camber and thickness ratios) and trimmed aircraft flight conditions. Calculates profile, wave and induced drag. Correction factors for interference drag are present.
3. Mission performance. Includes point performance calculations in climb, cruise and descent phases given user-set speed schedule, aircraft gross weight and altitude. Climb segment exit conditions can include a user-set altitude or an optimum altitude for best initial cruise range. The climb segment itself can be optimized for minimum time-to-climb or maximum range. Cruise segments can be defined by the user as flat cruise, climb cruise, or step cruise. Reserve segment calculations are also provided for hold and alternate airport flight segments. Taxi-in / out fuel consumption and low-speed takeoff / landing performance are also calculated.

1.3.2 VT MDO

Truss-braced wing preliminary aircraft design MDO at Virginia Tech stretches back almost two decades. An MDO framework was developed for truss-braced wing

aircraft studies in the late 1990's, with the concept showing much promise in studies for minimizing fuel and TOGW^{16,17}. A disadvantage to this early framework, however, was its existence as a large single code entity. Modifying individual pieces of the code (structures, aerodynamics, propulsion, etc.) was a painstaking process that made for an unwieldy piece of software. Furthermore, the optimization tool available was limited to a gradient-based solver that was inadequate to thoroughly explore the design space.

The current VT MDO framework uses Phoenix ModelCenter¹⁸ to provide an overall structure that is an improvement on the previous monolithic FORTRAN-based MDO code. The new framework with its component modules can be seen in flowchart form in Figure 3. While the logic and flow remains the same as in the old MDO code, the separation of the various components of the MDO process have allowed for easier modification and debugging of the code. Integration of the ModelCenter software environment also increases the optimizer options available and makes it more user-friendly. Users can easily view / update parameter inputs to the various modules, using a navigation toolbar similar to what PACELAB APD 3.1 provides. Unlike PACELAB, however, aircraft geometry cannot be viewed without the use of external software such as Vehicle Sketch Pad.

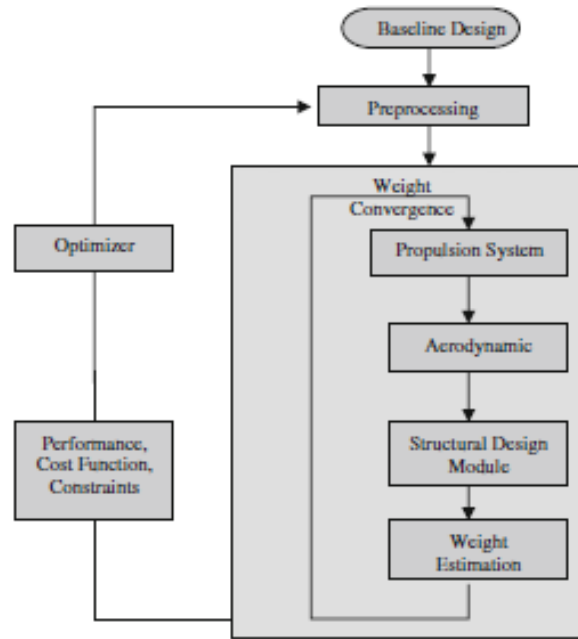


Figure 3. VT MDO Program Flow and Direction⁵

As can be seen in Figure 3, there are actually two loops within the VT MDO structure. The inner loop is for convergence of TOGW given a set of initial geometric design variables and flight conditions, iterating through the propulsion, aerodynamic, structural sizing and weight estimation modules, and then using the new estimated value of TOGW for the next iteration as an initial condition. Once TOGW converges, the aircraft mission performance is computed.

For propulsion system analysis, a simplified ‘rubber-engine’ model from work by Grasmeyer⁴ and Leiffson¹⁹, in turn based on a method from Mattingly⁴¹, is used to size the engine based on maximum sea level static thrust, as well as calculate fuel flow and thrust at altitude¹⁴. The aerodynamic performance is estimated based on various sources⁸, and is a large portion of the set of VT-based methods implemented in PACELAB-VT (see Chapter 2). The VT MDO structural design and weight estimation models uses a

combination of a double-plate FEM model for the wing bending material stiffness and weight and FLOPS equations for the rest of the structural and secondary weights⁵. Mission performance is calculated from a simplified mission profile with the Breguet range equation.

1.3.3 FLOPS

For the last few decades, FLOPS has been utilized extensively by NASA and research institutions across the United States as a preliminary design tool, and numerous studies have used it in the design process. Originally developed in 1984 by L.A McCullers of NASA LaRC in FORTRAN², FLOPS has been incrementally improved and expanded upon in the succeeding years by members of NASA. Its empirically based weight equations were developed in-house by NASA LaRC, and some are currently used by VT MDO as well, for estimating secondary wing weights.

Similar to both PACELAB and VT MDO, FLOPS is split among the various aerospace disciplines into individual modules. These modules can be replaced by user-written modules, the most attractive option to users who do not wish to involve themselves in the FLOPS source code. Instead of changing existing modules to fit their needs, they can simply replace entire modules with their own custom modules, provided the input / output parameters are the same. One of the advantages of FLOPS over default PACELAB and VT MDO is the ability to estimate aircraft noise and NO_x emissions.

FLOPS source code distribution / access is controlled by NASA LaRC and it is not typically distributed to entities outside of the United States. While some users may be given access to the source code and thus can expand or edit it as much as they desire, the lack of user-friendliness (there is no GUI, all files are text-based), and little technical

support outside of NASA LaRC, make this a difficult task. Documentation provides a summary of each module, as well as a list of all available parameters for the user to input as well as default values, but the learning curve is still quite steep for beginners. A version of FLOPS developed in conjunction with ModelCenter exists, but it was not used in this study²⁰. Thanks to extensive support from NASA LaRC, the default program was able to be used without incurring major time delays and was adequate for the work done here.

1.4 Wing Parameterization and Design Variables

Modifications made to PACELAB APD to incorporate physics-based methods for aerodynamics and wing structure are described in detail in Chapter 2. The general approach to the optimization design variables taken in this study was to vary the geometric parameters of the wing and strut, if present, as well as maximum sea level static thrust and cruise altitude. Fuselage and empennage parameters are fixed. This scheme reflects that used in past optimization studies at Virginia Tech⁵, where the emphasis has been on strut- or truss-braced wings. While parameters corresponding to these quantities exist in PACELAB and thus the two optimization approaches are very close, the available design variables in FLOPS are both fewer in number and more general in nature (e.g., total wing area as opposed to geometric properties of specific trapezoidal wing sections). Therefore, the similarity of the final aircraft in FLOPS is a rough one and is presented here to provide a comparison between a well-established traditional MDO program and the more recent codes that have been developed.

1.4.1 Wing Geometric Parameterization

PACELAB APD 3.1 and PACELAB-VT use a high-level parameterization scheme that involves defining the wing as two trapezoidal sections (i.e., a simple wing with a single ‘kink’) with each section being defined by its chord, geometric twist and thickness ratios at the cross-sections at both ends, as well as the 2-D airfoil data at those cross-sections. The quarter-chord sweep of the outer section is also a parameter, as is the wing dihedral, and leading edge sweep is constant along the wing (see Figure 4).

Figure 5 showcases the geometric parameters of the strut used in the PACELAB-VT framework. Because the strut component was ‘added’ to the data model in PACELAB APD 3.1 during this study, it is defined separately from the wing. Similar to the wing, the thickness and chord properties are defined at the centerline and tip.

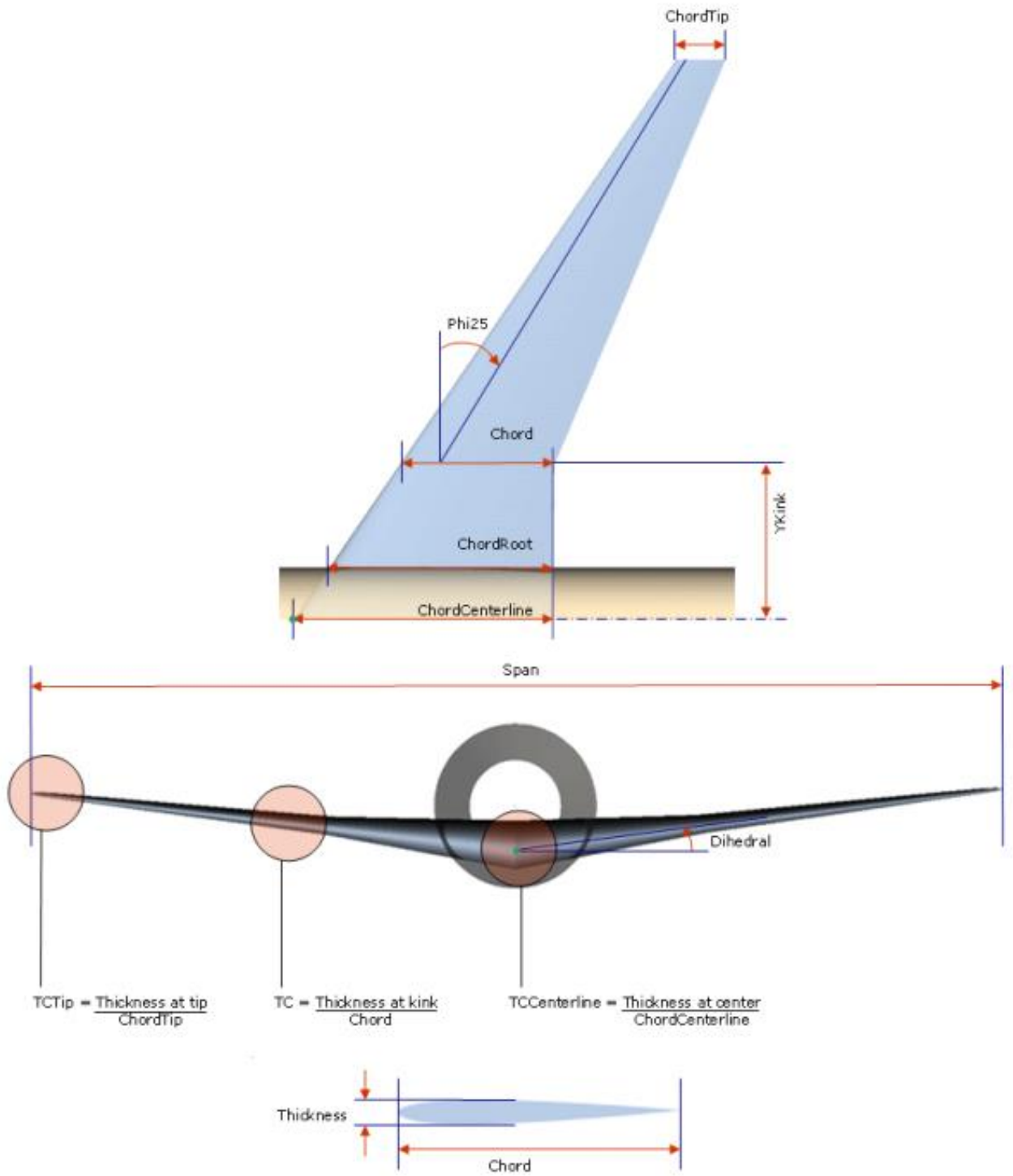


Figure 4. PACELAB APD 3.1 wing parameterization²¹

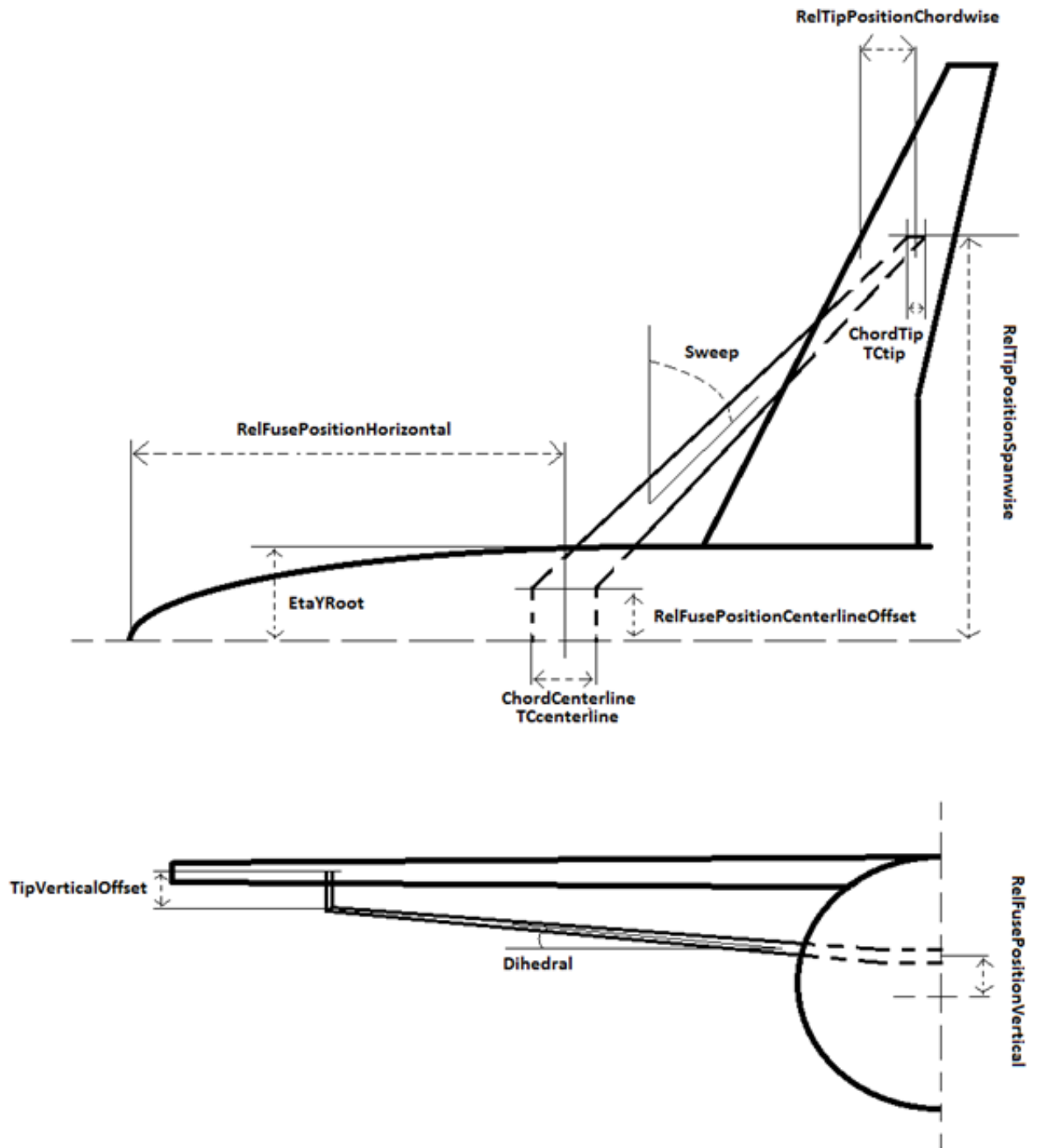


Figure 5. PACELAB-VT strut parameterization

VT MDO uses a RAGE-based geometry definition that consists of defining break point cross sections in the configuration's planar surfaces as well as their positions in 3-D space and any rotations of the cross-sections through the three Euler angles (see Figure 6), as well as their chord and thickness ratios.

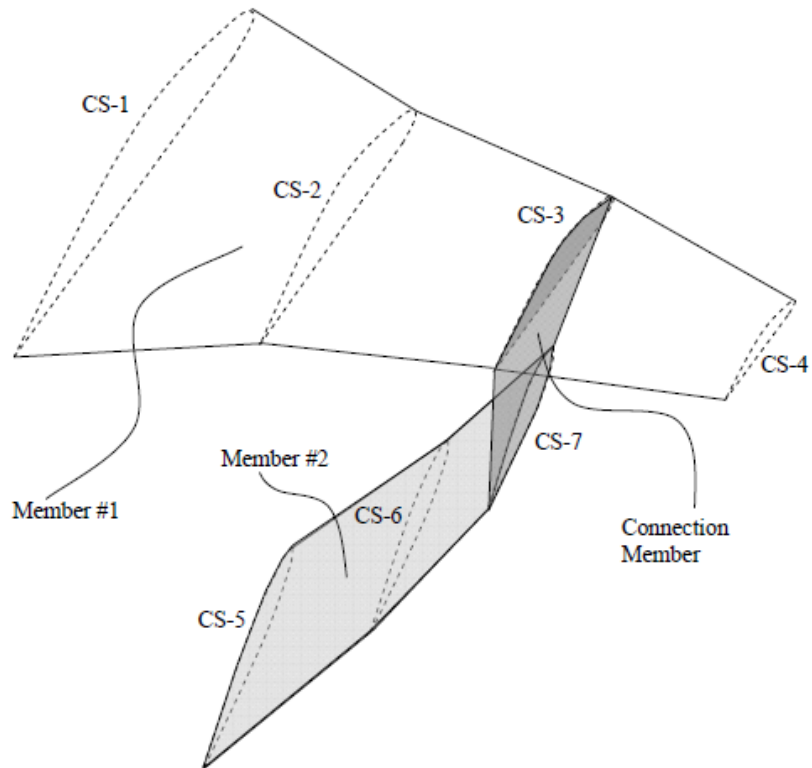


Figure 6. VT MDO planar surface parameterization²²

Sweep angles are then interpolated from the spatial positions of the cross-sections. This approach is more versatile and lower-level than that used in PACELAB as it allows for many different shapes and orientations of a wing, strut, or general planar surface type, while the PACELAB parameterization limits a wing to the given parameters in Figure 4.

Figure 7 shows what cross sections are defined in the VT MDO case for an SBW aircraft with wing-mounted engines (the configuration used in this study). In PACELAB

APD 3.1 and PACELAB-VT, by contrast, sweep angles are directly used as design variables for the wing sections, and cross-sections can only be rotated by specifying a wing twist at the centerline, kink and tip locations.

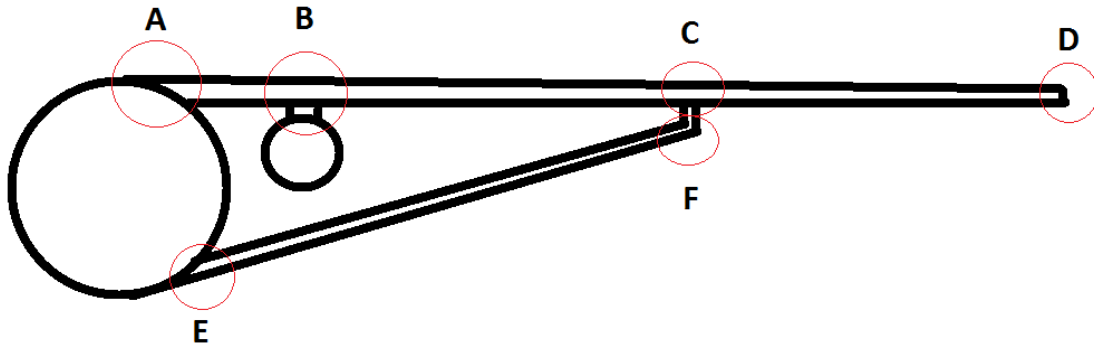


Figure 7. VT MDO defined cross sections

FLOPS wing parameterization utilizes two approaches. The first is an optional ‘detailed wing’ that defines thickness ratios, chord, and load path sweep of user-set break points in the wing. This is primarily for wing weight calculation, although it does refine wetted area and thickness ratio calculation for the aerodynamics. The second approach is the ‘general’ wing with two of three parameters user-specified: aspect ratio, area, or span, and these are utilized for the aerodynamic calculations along with taper ratio and a ‘weighted average’ thickness ratio for the wing.

1.4.2 Design Variables

Table 1 shows the optimization design variables (including the two non-geometric design variables) used in PACELAB-VT while Table 2 shows those used in VT MDO. Cantilever design variables are highlighted in black while additional variables introduced by the strut are highlighted in red (single strut, no juries). It should be noted that for

properties such as thickness ratios and chords that vary between cross-sections, a linear variation is assumed. This is true for both VT MDO and PACELAB-VT.

Looking at Figures 4 and 7 in conjunction with these tables, it can be seen that while the particular variables differ between the two frameworks, the same aircraft characteristics are actually being varied in the optimization. For example, varying the cross-section D x-coordinate in the VT MDO design is equivalent to varying wing quarter-chord sweep in PACELAB-VT.

Table 1. PACELAB-VT design variables (cantilever in black, SBW in red)

Wing centerline chord
Wing centerline thickness ratio
Wing kink chord
Wing kink thickness ratio
Wing tip chord
Wing tip thickness ratio
Wing span
Wing outer section quarter-chord sweep
Y-position of kink
Relative position of strut centerline along fuselage
Strut thickness ratio
Strut chord
Strut tip vertical offset distance
Maximum thrust
Cruise altitude

Table 2. VT MDO design variables (cantilever in black, SBW in red)

Cross-section A chord
Cross-section A thickness ratio
Cross-section C chord
Cross-section C thickness ratio
Cross-section C y-coordinate
Cross-section D x-coordinate
Cross-section D chord
Cross-section D thickness ratio
Cross-section E x-coordinate
Cross-section E chord
Cross-section E thickness ratio
Cross-section F z-coordinate

Maximum thrust
Cruise altitude

FLOPS design variables are more general than those in PACELAB-VT and VT MDO. For aircraft configurations that do not have detailed engine data available (i.e., an engine deck is input instead of generated) and with the optimization scheme presented here, the design variables are:

Table 3. FLOPS design variables (cantilever only)

Wing area
Wing aspect ratio
Wing sweep
Wing taper ratio
Wing thickness (weighted average)
Maximum thrust
Cruise altitude

To simplify the optimization problem, geometric constraints are also utilized in the wing geometry. For VT MDO, these constraints are shown in Table 4. Even with the difference between the two wing parameterizations, constraints are also able to be defined in PACELAB-VT such that the geometry is similarly constrained. Further geometric constraints and boundaries not listed here are also utilized to ensure a physically realistic design (such as mandating that the kink span-wise location be less than the tip).

Table 4. Wing geometric constraints

No dihedral
Chord across strut is constant
Thickness ratio across strut is constant
Strut tip y-location is locked to kink y-location

These geometric constraints are not definable in FLOPS except for the dihedral and are, therefore, unused in FLOPS for the results in the final part of this study.

1.5 Baseline Aircraft and Mission

The earliest MDO studies at Virginia Tech considered a long-range 777-like aircraft²³. Meadows¹⁴ was the first to perform an MDO study of a 737-like regional aircraft at Virginia Tech, and this study seeks to compare those results, generated from the VT MDO code, with new results generated with PACELAB APD 3.1 updated with VT MDO-based methods, which uses a mixture of those methods (aerodynamics, engine size / weight scaling, wing weight estimation) and the default PACELAB 3.1 methods (mission performance, propulsion).

The aircraft and its mission are represented by Figure 8. Important requirements include a minimum cruise range of 3,115 nm, a minimum TOFL of 8700 feet, approach speed of 142 knots, constant Mach cruises for both main and reserve segments (altitude is a design variable), reserve range of 200 nm, and a payload of 162 passengers (single-class). The baseline aircraft has a fuel load of 45300 lbs.

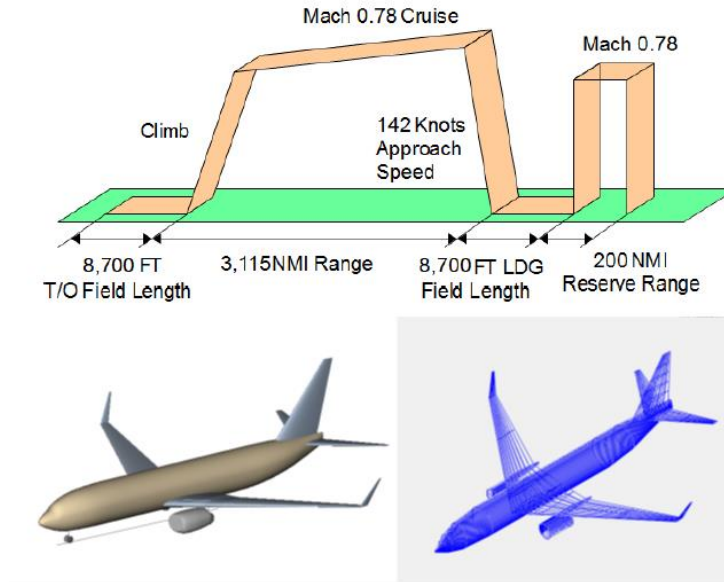


Figure 8. Mission profile and baseline aircraft¹⁴

These mission requirements are incorporated in the MDO process as a series of constraints (along with the geometric constraints, see Table 4) on the output parameters. Solutions that are outside constraint boundaries are not considered feasible solutions. The constraints on performance include:

- 1) Range is greater than 3,115 nautical miles with a 200 nautical mile reserve range
- 2) Cruise residual rate of climb is greater than 300 feet-per-minute
- 3) Two-dimensional maximum lift coefficient is less than 0.8, to ensure the airfoil is physically realistic in the transonic regime
- 4) Fuel required to complete the mission does not fill the tanks beyond their geometric capacity
- 5) To avoid wing scraping, wing tip deflection does not dip below the bottom of the fuselage during the 2 g taxi bump case (that is, the load case where maximum downward deflection on the ground would occur)

- 6) Second segment climb gradient is greater than 2.4% (FAR regulation)
- 7) Approach velocity of greater than $1.3V_{stall}$ (FAR regulation)
- 8) Landing distance satisfies FAR regulations
- 9) Missed approach climb gradient is greater than 2.1% (FAR regulation)

Because this study originated in work accomplished by Virginia Tech with the in-house MDO code, all these constraints are present in the VT MDO code. However, they may not necessarily have the ability to be implemented in the other software packages examined here. In the case of PACELAB-VT, one constraint is missing. The missed approach gradient requirement (an FAR regulation) is not present as there is no corresponding parameter present. This is also true for PACELAB APD 3.1, as well as the lack of the tip deflection constraint (wing deflection is not calculated in PACELAB APD 3.1). As for FLOPS, only constraints 1, 2, 4, 7 and 8 are definable in the optimization due to its more strictly defined optimization framework.

1.6 Optimization Frameworks

1.6.1 PACELAB APD 3.1 Optimization

Optimization in PACELAB is handled by first selecting some output parameter within the model for minimization and then specifying which input parameters to use for design variables. Constraints can be applied to these parameters (other than the boundaries specified within the optimizer), and non-design variable constraints can also be applied on the rest of the data model, as long as a corresponding parameter in the mathematical model exists for that constraint. This is why the single FAR constraint present in the MDO code (see Section 1.5) is not available in PACELAB APD 3.1 – a

corresponding parameter for this constraint does not exist in either the original software or the expansions performed in the course of this study.

PACELAB has three options to choose from for optimizers:

- Frontline Evolutionary (genetic algorithm)
- CONMIN (gradient-based solver)
- NLPQLP (sequential quadratic programming solver)

Users can specify options such as population sizes, constraint tolerances, and maximum iterations, which allows for a balance between accuracy and runtime.

The genetic algorithm, Frontline Evolutionary, is useful for conducting global searches of the configuration design space, and it is more dependent on the design space boundaries rather than the initial conditions. However, it does not utilize gradient information and is not guaranteed to find a global minimum by itself within any realistic amount of runtime. The algorithm stops when its population members have fitness values within a certain tolerance of each other, or when a time limit is reached, depending on user-set parameters. Much care must be taken to set realistic bounds on the design space, to keep candidate designs physically reasonable and prevent fatal errors from being encountered.

Conversely, the other two solvers, CONMIN and NLPQLP, utilize gradient information and thus converge upon local minima that are dependent on the starting conditions of the design variables, usually with faster runtimes than global-search solvers such as Frontline Evolutionary. Complex models such as those found in aircraft conceptual design have numerous local minima in their design space which puts gradient-

based solvers such as these at a significant disadvantage when they are used by themselves.

A compromise approach can be followed similar to current practice in VT MDO where the genetic algorithm is run a fixed number of times to sample different areas of the design space and generate initial conditions that are then used for a gradient-based solver to run on. This way, a global minimum is ‘approached’. There is no guarantee, of course, that this would be the global minimum because that would require an infinite runtime for the algorithm.

This approach is what was used to generate the last set of results in this study, where minimum-fuel optimizations for cantilever and strut-braced wing aircraft were performed, by utilizing Frontline Evolutionary followed by CONMIN. This gives a more comprehensive exploration of the design space than usage of a gradient-based solver alone and is especially useful for nonconventional design spaces such as that for a SBW aircraft.

1.6.2 VT MDO Optimization

Recall from Figure 3 that the VT MDO code contains two loops. The outer loop is the main optimizer which within the ModelCenter environment can utilize a ‘hybrid’ optimization scheme involving the usage of a global-search scheme (ModelCenter’s own Darwin²⁴ genetic algorithm) to give a gradient-based solver (Vanderplaat or ModelCenter’s Design Optimization Tool) several ‘candidate’ portions of the design space in which local minima can then be found.

This hybrid approach is taken to prevent extremely long runtimes (on the order of days) when running Darwin with a full set of design variables for a strut- or truss-braced

aircraft. The loop-within-a-loop structure of VT MDO additionally increases the runtime. Running the gradient solvers alone reduces the runtime down to a matter of hours but this, of course, takes away the global-search capability.

1.6.3 FLOPS Optimization

Optimization in FLOPS is handled by minimization of a single objective function in which each term is representative of some desired characteristic to be minimized.

Table 5 shows the characteristics that are available for minimization.

Table 5. FLOPS configuration characteristics available for minimization or maximization

Ramp weight
Fuel mass
Cruise Mach number x lift-to-drag ratio
Range
Life cycle cost
Specific fuel consumption
NOx emissions
Flyover noise
Sideline noise
Noise figure of merit
Hold time for hold segment of mission

Each term is also multiplied by a user-set weighting factor, which allows for more or less emphasis to be placed on a particular characteristic as desired. For a min-fuel optimization such as that performed in this study, all weighting factors except that for fuel are set to zero.

Choices for optimization algorithms in FLOPS are limited to a number of local search methods, which means that the optimization results are dependent on the initial aircraft parameters. These methods include:

- Davidon-Fletcher-Powell (DFP) Algorithm

- Broyden-Fletcher-Goldfarb-Shano (BFGS) Algorithm
- Conjugate Gradient (Polak-Ribiere) Algorithm
- Steepest Descent Algorithm
- Univariate Search Algorithm
- Kreisselmeier-Steinhauser function with DFP Algorithm

For the work presented here, the default option (BFGS) was utilized. Other choices were experimented with and it was found that, generally, BFGS was the most robust and had the best convergence behavior.

CHAPTER 2: Physics-Based Modifications to PACELAB APD

In this chapter, a detailed description of the physics-based VT MDO methods added in PACELAB APD 3.1 during the course of this study is given, as well as the validation process utilized to verify the methods were correctly implemented. As stated in the introduction, these physics-based methods were added to default PACELAB APD 3.1 for improved fidelity and so that unconventional configurations can be studied.

Validation of the aerodynamic methods involved three distinct physical models for verification that the method had been implemented properly. The engine scaling model was simple enough that merely evaluating engine weight / dimensions resulting from the single input parameter (maximum thrust) was sufficient for validation. The structural model was validated by comparing bending stiffness across the wing between the critical bending stiffness (load limit), the VT MDO calculated stiffness, and the calculated stiffness from the new method. These models and their validation results are discussed after the method descriptions in the following sections.

2.1 Aerodynamic Models

The primary advantage of the new aerodynamic models⁸ for profile, wave and interference drag from VT MDO added to PACELAB APD 3.1, over the existing empirical methods from Torenbeek⁶ and Raymer¹, is the consideration of the exposed surfaces as a series of ‘strips’ with individual drag components of each strip summed to provide the overall drag coefficient for the surface. Another important advantage is a more accurate semi-empirical estimation of drag in the transonic regime thanks to the inclusion of the Korn Equation for wave drag (see Section 2.1.3) extended for swept wings, an improvement over the simple interpolation between supersonic and subsonic

drag that the default PACELAB method uses, based on an approximation from Raymer¹. Further improvements include the use of a CFD-based method developed by Tetrault²⁵ to actually calculate interference drag instead of just using ‘correction factors’. For profile drag, a method for transition calculation is added that takes into account the airfoil technology level (i.e., the presence of natural laminar flow, or NLF technology) and calculates transition at each strip location instead of the entire surface.

2.1.1 Induced Drag

For the work in this study, the default PACELAB APD 3.1 methods for induced drag were deemed adequate for the analysis of the proposed aircraft configuration. This is due to the assumption of non-lifting struts on the aircraft, hence from the perspective of the induced drag the aircraft is a ‘conventional’ configuration, and the existing PACELAB APD 3.1 induced drag method is adequate for this work.

PACELAB APD 3.1 (and PACELAB-VT) induced drag calculation comes from two methods – a subsonic method based on empirical data, developed by Torenbeek⁶ and a supersonic method from Raymer¹. In the transonic regime, a simple interpolation between the two results is performed.

For the subsonic method, induced drag coefficients for both the wing and tail are based on the familiar C_L^2 equation²⁶:

$$C_{D,i} = \frac{C_L^2}{\pi e AR} \quad \text{Eqn. 1}$$

For the wing, efficiency is estimated based on taper ratio of the main planform, using an empirical method developed by Diederich (Equation F-16 of Torenbeek⁶). The method does not directly calculate the lift distribution on the wing, only the span

efficiency factor. Therefore, for the purpose of calculating the wave and interference drag with the new implemented methods (Sections 2.1.3 and 2.1.4), a distribution shape must be assumed. Another important limitation of the method is that any winglet effects on induced drag are not directly calculated, rather PACELAB-VT simply has a user-set calibration parameter to represent the winglet ‘benefit’, in the form of a percentage reduction in wing induced drag coefficient. This does not impact the current study as the aircraft configuration used here does not have winglets. A simple correction factor for wing twist, if present, is also applied (Equation F-20, Torenbeek⁶). For the tail, a ‘deviation’ from the elliptical case by an increment of 2% is assumed.

A useful inclusion in the PACELAB-VT induced drag is a simple estimation of fuselage induced drag. This does have a significant impact on the calculated induced drag coefficient.

For more discussion on the impact of an assumed lift distribution and the induced drag calculation on the fuselage for a full aircraft configuration, see Section 2.1.5.2.

2.1.2 Profile Drag

Profile drag calculation in the VT MDO method consists of a combination of friction drag with an equivalent flat plate model and form (pressure) drag using “form factors” as correction terms applied to the friction drag coefficient. Planar surfaces such as wings, stabilizers and canards are divided into stream-wise strips, and the profile drag is calculated separately for each strip. Bodies such as nacelles and fuselages, and planar surfaces that carry no lift such as pylons and vertical fins are handled as single entities.

Planar surfaces are characterized in PACELAB-VT by leading and trailing edge sweep, as well as span and chord lengths at specific points (centerline, root, kink and tip).

Cross sectional information such as thickness ratios are also known at these points. For strip calculations on a given surface, a trapezoidal section is considered. For each trapezoidal section, 50 strips are used. There are two of these sections for the wing, inboard and outboard of the kink point, and one section for other surfaces. For each of these sections, strip widths, strip lengths and wetted areas can be calculated, as shown in Equations 2 – 4. In Equations 3 and 4, “i” runs from 1 to the total number of strips in the section.

$$StripWidth = \frac{SectionWidth}{50} \quad Eqn. 2$$

$$StripLength^i = \frac{1}{2}(i \cdot StripWidth \cdot \tan \Lambda_0 - i \cdot StripWidth \cdot \tan \Lambda_{1,0}) + \frac{1}{2}((i - 1) \cdot StripWidth \cdot \tan \Lambda_0 - (i - 1) \cdot StripWidth \cdot \tan \Lambda_{1,0}) \quad Eqn. 3$$

$$Swet^i = 2 \times StripLength^i \times StripWidth / \cos dihedral \quad Eqn. 4$$

Equation 2 gives the strip length down the middle of the strip (average of inboard and outboard lengths). Note the division by the cosine of the dihedral in Equation 3 – this is done because the strip widths are only for the projected span. Actual widths, needed for wetted area calculation, are calculated by dividing by the dihedral cosine.

For both surface types, friction drag is modeled using a combination of laminar and turbulent flow models with an option for either a fixed transition point, or a transition point based on leading edge sweep and an airfoil technology factor (TF). The resulting coefficient is corrected with form factors for pressure drag, several forms of which are available for both planar surfaces and bodies of revolution. Change in profile drag due to lift is small and is neglected.

The profile drag module consists of several parameters that must be set by the user. These parameters are summarized in Table 6.

Table 6. Profile drag user-set parameters

BodyFormFactor	Specifies form factor type to use for all bodies
BodyTransitionRe	Specifies transition Re number for all bodies
FuselageRibletFactor	Factor applied to turbulent skin friction coefficient, simulates presence of ‘riblets’ on the fuselage to reduce turbulent skin friction. Default is 0.95
MaxLaminarFlow	Specifies decimal fraction amount of maximum allowable laminar flow for planar surfaces, acts as either a fixed transition point for planar surfaces or the limiting case for transition point calculated from wing sweep and technology factor, dependent on the user-set value of TransitionSwitch. Equivalent to transition location as a fraction of chord, and the ratio of transition Reynolds number to Reynolds number based on chord.
TechnologyFactor (TF)	Wing tech factor used in transition calculation where 0 represents natural laminar flow on traditional wings and 1 a natural laminar flow (NLF) airfoil
TransitionSwitch	Specifies whether MaxLaminarFlow is the transition point or the limiting case (when transition is calculated)
WingFormFactor	Specifies form factor type to use for all planar surfaces

The profile drag calculation for each strip or body can be summarized as five major steps:

- Calculate transition using TF, with MaxLaminarFlow as the limiting value for laminar flow (or directly apply MaxLaminarFlow as the transition point, depending on the TransitionSwitch setting, and ignore TF)
- Calculate skin friction coefficient
- Calculate form factor
- Calculate profile drag coefficient
- Scale profile drag coefficient by ratio of wetted area to reference area

The following subsections detail each of these steps.

2.1.2.1 Transition Calculation

“Transition” as used in the method is defined as “decimal fraction of chord of the flow over a surface that is laminar”. This is also the relative transition location on a surface, and the ratio between transition Re number and Re number based on the surface reference length. These relationships are summarized in Equation 4.

$$Transition = \frac{\textit{laminar flow}}{\textit{turbulent flow}} = \frac{X_{\textit{trans}}}{\textit{Length}} = \frac{Re_{\textit{trans}}}{Re_L} \quad \text{Eqn. 5}$$

If the user-set parameter TransitionSwitch is selected in Engineering Work Bench, a drop-down menu appears that gives two choices: “FixedPoint” and “Calculated”. The first option will use the user-set value of MaxLaminarFlow as the transition location (as x / L where L is the length of the component) for planar surfaces. The second option will calculate the transition location for planar surfaces based on leading edge sweep and the user-set parameter TechnologyFactor. For bodies, transition is calculated from the user-set parameter BodyTransitionRe.

Calculation of transition for planar surfaces is based on a simple model developed from work by Braslow²⁷ as a function of leading edge sweep and technology factor (see Figure 9). If surface strips are being used (wings, stabilizers and canards) this calculation is performed for each strip. Other planar surfaces (pylons and fins) only have this calculation performed once. This calculation is only applicable to planar surfaces and is not applied to bodies. For surfaces with technology factors between 0 and 1, the transition Re number is interpolated from the curves in Figure 9. If MaxLaminarFlow is set to less

than 1 but greater than zero, calculated transition is capped at MaxLaminarFlow, if it is greater than MaxLaminarFlow.

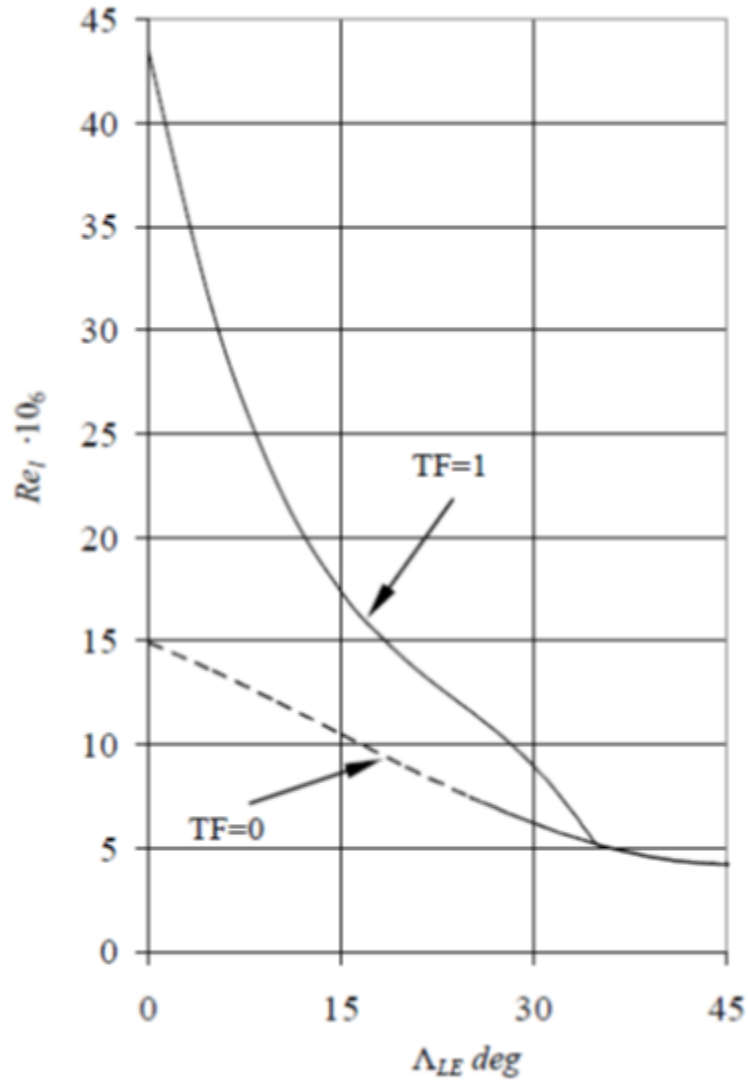


Figure 9. Transition calculation based on technology factor and leading edge sweep⁸

Once transition is known, checks are performed to ensure that the transition is not greater than 1 (fully laminar) and is not 0 (fully turbulent). Cases that are greater than 1 are capped at 1 to prevent non-physical results and cases at 0 are increased to a small value above zero (10E-5) to prevent divide-by-zero errors later in the method.

2.1.2.2 Skin Friction Coefficient Calculation

For each strip, surface or body, skin friction coefficient is calculated for both laminar and turbulent cases, and then a composite coefficient is formulated from the transition location. Each calculation step is summarized below. For laminar and turbulent skin friction coefficients at subsonic Mach numbers, the results are not sensitive to edge temperature so this can be considered a fixed parameter.

Laminar skin friction at a point on a surface (x) is computed from the Blasius formula²⁶ with a compressibility correction using the Eckert Reference Temperature Method²⁸. Variables are defined in Table 7. The assumptions and equations used are summarized in Table 8.

Table 7. Laminar skin friction variables

Variable Name	Definition
T_w	Wall temperature
T_e	Boundary layer edge temperature
T_{AW}	Adiabatic wall temperature
r	Recovery factor
Pr	Prandtl number
γ	Gamma, specific heat ratio
M_e	Mach number of boundary layer edge (freestream)
T^*	Reference temperature
C^*	Chapman-Rubesin constant
K	Constant for Sutherland's Law
C_f	Laminar skin friction coefficient
Re_x	Freestream Reynolds number based on x
C_F	Total laminar skin friction coefficient

Table 8. Laminar skin friction formulas

Formula	Comments
	Wall temperature to edge temperature ratio. Assumptions: $Pr = 0.72$

$\frac{T_w}{T_e} = \frac{T_w}{T_{AW}} \left(1 + r \frac{\gamma - 1}{2} M_e^2 \right)$	$r = \sqrt{Pr}$ $\gamma = 1.4$ $T_e = 390 \text{ deg } R$ $\frac{T_w}{T_{AW}} = 1.0$
$\frac{T^*}{T_e} = 0.5 + 0.039 M_e^2 + 0.5 \left(\frac{T_w}{T_e} \right)$	Reference temperature ratio.
$C^* = \sqrt{\frac{T^*}{T_e} \left(\frac{1 + K/T_e}{\frac{T^*}{T_e} + K/T_e} \right)}$	C-R constant based on reference temperature and Sutherland's viscosity law. Assumptions: $K = 200 \text{ deg } R$
$C_f = \frac{0.664 \sqrt{C^*}}{\sqrt{Re_x}}$	Blasius formula with C-R constant.
$C_F = 2C_f$	Integration of Blasius formula from zero up to x

Turbulent skin friction at a point on a surface (x) is calculated from the “Van Driest II” method from a recommendation by Hopkins and Inouye²⁹. The specific algorithm used is taken from further work by Hopkins³⁰. Variable definitions are referenced in Table 9, while assumptions and equations are summarized in Table 10.

Table 9. Turbulent skin friction variables

Variable Name	Definition
γ	Gamma, specific heat ratio
M_e	Mach number of boundary layer edge (freestream)
T_w	Wall temperature
T_e	Boundary layer edge temperature
T_{AW}	Adiabatic wall temperature
r	Recovery factor
$m, F, A, B, \alpha, \beta, F_c, F_\theta, F_x$	Intermediate variables
Re_x	Freestream Reynolds number based on x
\overline{Re}_x	Reynolds number based on x (incompressible)
\overline{C}_F	Total laminar skin friction coefficient (incompressible)
C_F	Total laminar skin friction coefficient

Table 10. Turbulent skin friction formulas

Formula	Comments
$m = \frac{\gamma - 1}{2} M_e^2$	Calculation of intermediate variable m. Assumptions: $\gamma = 1.4$
$\frac{T_{AW}}{T_e} = 1 + rm$	Calculation of $\frac{T_{AW}}{T_e}$. Assumptions: $r = 0.88$
$F = \frac{T_w}{T_e} = \frac{T_w}{T_{AW}} \frac{T_{AW}}{T_e}$	Calculation of intermediate variable F. Assumptions: $\frac{T_w}{T_{AW}} = 1.0$ $T_e = 222 \text{ K}$
$T_w = F \cdot T_e$	Calculation of wall temperature.
$A = \left(\frac{rm}{F}\right)^{1/2}$	Calculation of intermediate variable A.
$B = \frac{1 + rm - F}{F}$	Calculation of intermediate variable B.
$\alpha = \frac{2A^2 - B}{(4A^2 + B^2)^{1/2}}$	Calculation of intermediate variable α .
$\beta = \frac{B}{(4A^2 + B^2)^{1/2}}$	Calculation of intermediate variable β .
$F_c = \frac{rm}{(\sin^{-1} \alpha + \sin^{-1} \beta)^2}$	Calculation of intermediate variable F_c if $M_e > 0.1$
$F_c = \left(\frac{1 + \sqrt{F}}{2}\right)^2$	Calculation of intermediate variable F_c if $M_e \leq 0.1$
$F_\theta = \sqrt{\frac{1}{F} \left(\frac{1 + \frac{122}{T_w} \times 10^{-5/T_w}}{1 + \frac{122}{T_e} \times 10^{-5/T_e}} \right)}$	Calculation of intermediate variable F_θ (Keyes viscosity law).
$F_x = \frac{F_\theta}{F_c}$	Calculation of intermediate variable F_x .
$\overline{Re}_x = F_x Re_x$	Calculation of incompressible Reynolds number.
$\frac{0.242}{\sqrt{C_F}} = \log(\overline{C_F} \overline{Re}_x)$	Calculation of incompressible skin friction coefficient. Solve with Newton's method.....

$\overline{C}_F^{i+1} = \overline{C}_F^i \left[1 + \frac{0.242 - \sqrt{\overline{C}_F^i} \log(Re_x \overline{C}_F^i)}{0.121 + \sqrt{\overline{C}_F^i} / \ln 10} \right]$	Newton's method applied to incompressible skin friction coefficient equation. Solve with initial guess of $\overline{C}_F^0 = \frac{.074}{Re_x^{0.2}}$.
$C_F = \frac{\overline{C}_F}{F_C}$	Calculation of total turbulent skin friction coefficient.

Composite skin friction coefficient based on transition location is calculated from Schlichting's Composite Formula³¹ as shown in Equation 5.

$$C_F = C_{F_{TURB}}(Re_L) - \left(\frac{x_{trans}}{L}\right) [C_{F_{TURB}}(Re_{trans}) - C_{F_{LAM}}(Re_{trans})] \quad \text{Eqn. 5}$$

See Equation 4 and Section 2.1.2.1 for the relationships between the Reynolds numbers and transition location.

2.1.2.3 Form Factor Calculation

Corrections to the friction drag to account for pressure drag are applied with form factors for both planar surfaces and bodies. User-set parameters WingFormFactor and BodyFormFactor determine which form factor type to use for each of these cases, respectively. Selecting these parameters brings up a drop-down box with the various form factor names that are available. Table 11 lists the geometric variables that are used in form factor calculation. Table 12 lists the various form factors available and their equations.

Figure 10 shows comparisons between the various form factor types available.

Table 11. Form factor variables

Body Form Factors (Parameter BodyFormFactor)	
Variable	Definition
$\frac{l}{\bar{d}}$	Fineness ratio
Planar Form Factors (Parameter WingFormFactor)	
Variable	Definition

Λ_x	Surface sweep at chordwise location x
t/c	Thickness ratio
M_∞	Mach number

Table 12. Form factor options and formulas

Body Form Factors (Parameter BodyFormFactor)	
Formula	Comments
$FF = 1.0 + \frac{1.5}{\bar{d}} \frac{l}{l^{1.5}} + \frac{7.0}{\bar{d}} \frac{t}{l^{3.0}}$	Hoerner ³⁵ form factor
$FF = 1.0 + \frac{2.2}{\bar{d}} \frac{l}{l^{1.5}} + \frac{3.8}{\bar{d}} \frac{t}{l^{3.0}}$	Torenbeek ⁶ form factor
$FF = 1.0 + \frac{2.8}{\bar{d}} \frac{l}{l^{1.5}} + \frac{3.8}{\bar{d}} \frac{t}{l^{3.0}}$	Shevell ³⁹ form factor
$FF = 1.0 + .0025 \frac{l}{\bar{d}} + \frac{60.0}{l^{3.0}}$	Raymer-Jobe ³² form factor
Planar Form Factors (Parameter WingFormFactor)	
Formula	Comments
$FF = 1.0 + 2.0 \frac{t}{c} + 60.0 \left(\frac{t}{c}\right)^4$	Hoerner ³⁷ form factor
$FF = 1.0 + 2.7 \frac{t}{c} + 100.0 \left(\frac{t}{c}\right)^4$	Torenbeek ⁶ form factor
$FF = 1.0 + \frac{(2 - M_\infty^2) \cos \Lambda_{0.25}}{\sqrt{1 - M_\infty^2 \cos^2 \Lambda_{0.25}}} \frac{t}{c} + 100.0 \left(\frac{t}{c}\right)^4$	Shevell ³⁹ form factor
$FF = \left(1.0 + 2.0 \frac{t}{c} + 100.0 \left(\frac{t}{c}\right)^4\right) (1.34 M_\infty^{0.18} \cos^{0.28} \Lambda_{0.5})$	Nicolai-Raymer ¹ form factor
$FF = 1.0 + 1.8 \frac{t}{c} + 50.0 \left(\frac{t}{c}\right)^4$	Grumman ⁸ form factor

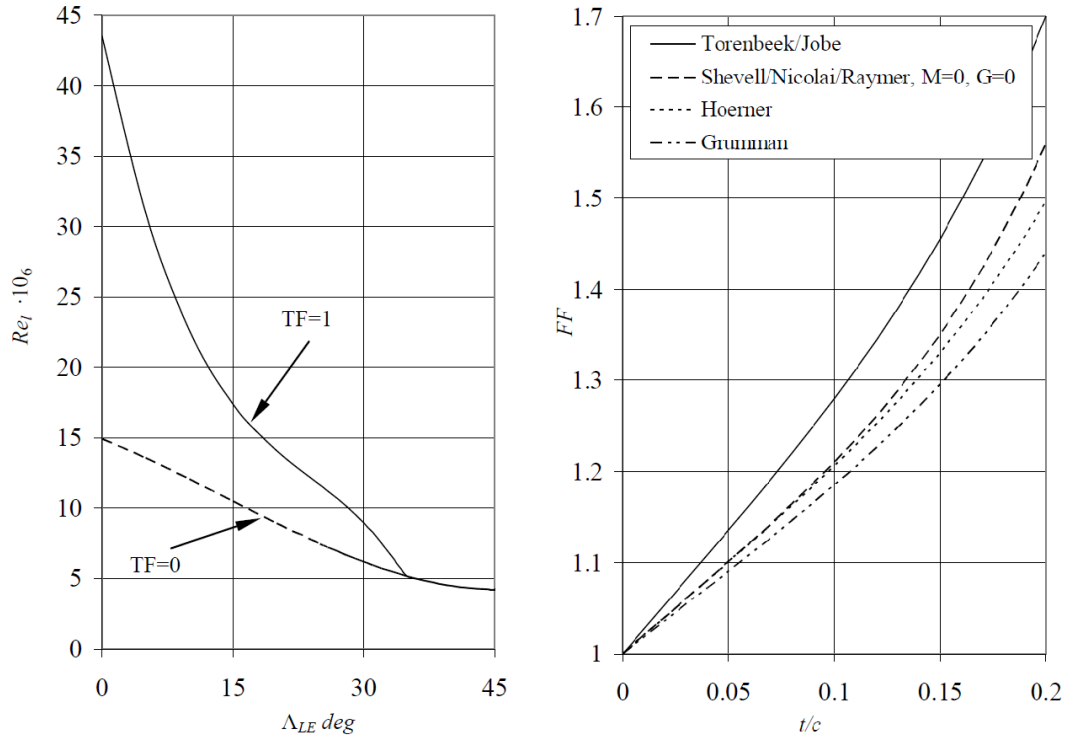


Figure 10. Differences in planar and body form factors⁸

2.1.2.4 Profile Drag Coefficient Calculation

Once composite skin friction coefficient and form factors are known, unscaled profile drag coefficients are then calculated from Equation 6.

$$C_{d,F} = C_F \cdot FF \quad \text{Eqn. 6}$$

However, the profile drag calculation is incomplete as the drag coefficients still need to be properly scaled by area.

The final step in calculating the profile drag for a component is scaling the coefficient by the ratio between component wetted area and reference area as in Equation 7.

$$C_{D,F} = C_{d,F} \cdot \frac{S_{wet}}{S_{ref}} \quad \text{Eqn. 7}$$

For components that are treated as one unit this is a simple matter of just using the PACELAB-calculated wetted area and dividing by the aircraft reference area. However, for strip calculations on planar surfaces (wings, winglets, canards and stabilizers) the component must first be divided into the appropriate number of strips and then the profile drag of each strip is calculated and summed to provide the overall component profile drag coefficient. Profile drag is estimated for every aircraft section that is exposed to the freestream (unlike wave and interference drag, which apply only to planar surfaces and lifting surfaces, respectively).

2.1.3 Wave Drag

The wave drag computation in the VT MDO methods calculates the wave drag for each strip of each planar surface, utilizing Locke’s model for drag rise^{33,34} (see Table 15) and the Korn equation³⁵, which utilizes a user-set parameter specifying the ‘supercriticality’ of the airfoil (see Table 13).

Table 13. Wave drag user input parameter

AirfoilTechLevel	Ranges from 0.87 to 0.95, specifies ‘supercriticality’ of airfoil. Higher values reduce the wave drag.
------------------	--

This equation has been extended with simple sweep theory^{8,35}. Only one user-set parameter is required. For each strip, local lift coefficient factors into the calculation, therefore the lift distribution shape across the lifting surface must be known or assumed. For the work in this study, the VT MDO induced drag method was not added. It was deemed adequate that for cantilever airplanes, as well as an SBW configuration with a non-lifting strut, an elliptical distribution could be assumed. PACELAB APD 3.1 default methods³⁶ assume a span efficiency based on taper ratio, but it was found during

experimentation with the source code that this deviated only slightly from the elliptical case. From a given overall surface lift coefficient and elliptical distribution the section lift coefficients along the span needed for wave drag calculation can be derived.

Lifting surfaces are considered with a strip-by-strip approach, similar to the profile drag calculation. Non-lifting planar surfaces are considered as single components. Calculation of the wave drag consists of three major steps.

- Calculation of section lift coefficient using the elliptical lift distribution assumption
- Calculation of the sectional wave drag coefficient
- Scaling the drag coefficient by ratio of strip or surface area to reference area

The final step is identical to that for profile drag (see Section 2.1.2) with the exception that the strip area is now only considered to be one side of the strip. Therefore, it will not be discussed in detail here. The first two steps are discussed in further detail next.

To calculate the section lift coefficients, an elliptical lift distribution is assumed.

For a given ellipse the area under the curve is $\frac{1}{4}\pi ab$. The equation of the line is

$$\frac{x^2}{b^2} + \frac{y^2}{a^2} = 1 \quad \text{Eqn. 8}$$

By the definition of total lift coefficient for a trapezoidal wing shape,

$$C_L = \int_0^1 \frac{cc_L}{c_{avg}} d\eta \quad \text{Eqn. 9}$$

Here, c_{avg} is defined as $\frac{WingArea}{Span}$ and η is the relative span-wise location, ranging from 0 to

1. If an elliptical shape for $\frac{cc_L}{c_{avg}}$ (y in Equation 8) is desired, the value of b will be 1. This

is because x is equivalent to η and runs from 0 to 1. From the definition of an elliptical area and Equation 9:

$$C_L = \frac{1}{4}\pi a \implies a = \frac{C_L}{\pi/4} \quad \text{Eqn. 10}$$

Combining Equation 10 with Equation 8 and solving for y (or rather, $\frac{cc_l}{c_{avg}}$) gives

$$\frac{cc_l}{c_{avg}} = \frac{C_L}{\pi/4} \sqrt{1 - \eta^2} \quad \text{Eqn. 11}$$

Considering that at each strip along the wing the value of c will just be the calculated strip length, Equation 11 can be rearranged to give the 2-D lift coefficient at the center of strip “ i ”:

$$\frac{cc_l}{c_{avg}} = \frac{C_L}{\pi/4} \sqrt{1 - \eta^2} \quad \text{Eqn. 12}$$

Now that section lift coefficient at each strip is known, the rest of the wave drag calculation can proceed.

Table 14 defines the variables used in the calculation of wave drag coefficient. Table 15 summarizes the steps taken for calculation of wave drag coefficient for each strip or surface.

Table 14. Wave drag variables

Variable Name	Definition
$C_{d,w}$	Wave drag coefficient (unscaled)
M_{DD}	Drag divergence Mach number
M_{cr}	Critical Mach number
M_∞	Freestream Mach number
$\Lambda_{0.5}$	Half-chord sweep
κ_A	Technology factor, corresponds to user-set parameter AirfoilTechLevel
$\frac{t}{c}$	Thickness ratio
c_l	Local 2-D lift coefficient

Table 15. Wave drag formulas

Formula	Comments
$M_{DD} \cdot \cos \Lambda_{0.5} + \frac{c_l}{10 \cos^2 \Lambda_{0.5}} + \frac{\frac{t}{c}}{\cos \Lambda_{0.5}} = \kappa_A$	Korn equation ³⁵ , solved for drag divergence Mach number. Thickness ratio is linearly interpolated, similar

	to profile drag calculation. If component is non-lifting the entire surface is taken into account as one unit and section lift coefficient is 0.
$M_{cr} = M_{DD} - \sqrt[3]{\frac{0.1}{80}}$	Calculation of critical Mach number, taken from a definition in Gur et al ¹⁸ .
$C_{d,w} = \begin{cases} 0 & \text{if } M_{\infty} \leq M_{cr} \\ 20(M_{\infty} - M_{cr})^4 & \text{if } M_{\infty} > M_{cr} \end{cases}$	Calculation of wave drag coefficient (unscaled) from Locke's 4 th Power Law.

Once the unscaled wave drag coefficient is calculated it is scaled by the area ratio as explained in Section 2.1.2. Wave drag is calculated for all planar aircraft sections; wave drag on bodies is neglected.

2.1.4 Interference Drag

Interference drag for wing-body, strut-body, strut-wing, and strut-strut intersections is estimated using an interpolation between Hoerner's model³⁷ for high thickness ratios ($TC > 0.4$) and Tetrault's CFD model²⁵ for low thickness ratios ($TC < 0.075$). The intersection angle between the members is also calculated and factors into the overall interference drag calculated. For wing-fuselage (or stabilizer-fuselage) intersections, the intersection angle is considered to be the inclination of the wing to the fuselage surface normal (Figure 11).

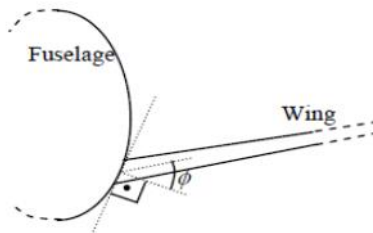


Figure 11. Wing-fuselage intersection angle¹⁴

This process is completed twice, once for the wing and again for the empennage. Similar to the wave drag computation, a single user-input parameter is needed: a junction ‘fairing factor’ that reduces the interference drag due to the presumed use of fairings, see Table 16.

Table 16. Interference drag user-set parameter

FairingFactor	Factor applied to overall interference drag coefficient, default is 0.1.
---------------	--

Calculation of interference drag can be split up into three main steps:

- Calculation of intersection angle
- Calculation of Hoerner interference drag coefficient
- Calculation of Tetrault interference drag coefficient
- Interpolation between the two methods for intermediate thickness ratios

The following sections explain these individual steps in more detail.

Given a cross-sectional slice of the fuselage at an intersection between a wing-like surface and the fuselage, as a list of points in 2-D space, the angle between the wing surface line and the fuselage surface normal can be approximately calculated. This is done by iterating around the fuselage cross-section point-list on one side (starting from the top of the cross-section) until two points on each side of the wing line are found (see Figure 12). In the second step, the equation of the line between these two points is found, and from this equation the surface normal is found. The angle between the wing line and the surface normal line is then calculated from simple trigonometry, and this is considered to be the inclination angle.

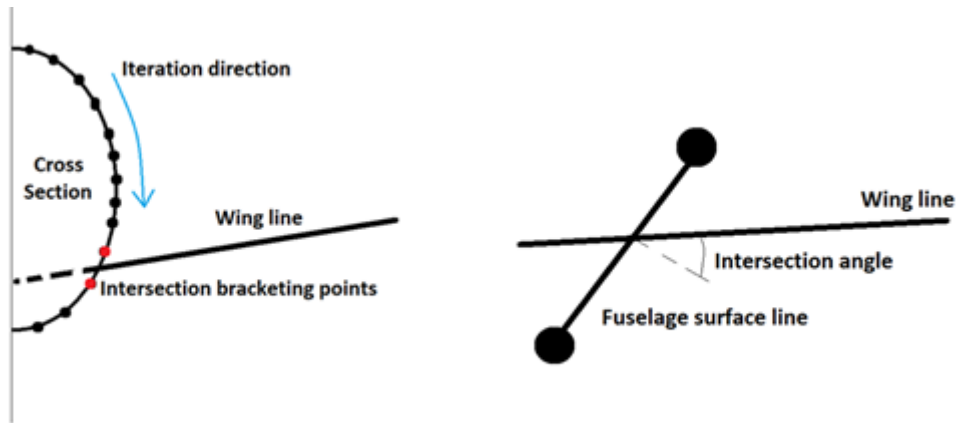


Figure 12. PACELAB inclination angle calculation

This algorithm ‘defaults’ to setting the inclination angle at the given surface dihedral if no solution is found; that is, the given surface does not intersect the fuselage. This is appropriate for T-tail configurations, where the stabilizer root intersects the vertical fin and not the fuselage.

While this method is an approximation from a point-list and thus not as accurate as calculating the angle from a continuous function describing the cross-section, its advantage comes from its ability to calculate the intersection angle for any cross-section that is provided as a list of points (allowing for advanced users to ‘import’ their own cross-sections). Accuracy can also be increased simply by increasing the number of points used in generating the point-list of the cross-section. In areas of the fuselage that do not have a constant cross-section down the length (such as the nose and tail areas) PACELAB-VT fuselage parameterization does not use smooth functions to describe the cross-sections, rather a user-set pointlist is used, making this approach necessary anyway.

Hoerner’s model³⁷ is applicable to intersection thickness ratios greater or equal to 0.4. This is much thicker than most wing or wing-like structures, hence the need for an

additional model (Tetrault²⁵). Table 17 defines the important variables in the method. Lift coefficient at the intersection is calculated with Equation 12 (see Section 2.1.3). Table 18 summarizes the formulas and steps associated with Hoerner’s method.

Table 17. Variables for Hoerner model

Variable Name	Definition
$\frac{t}{c}$	Average thickness ratio of intersecting members (for fuselage intersections, just the thickness ratio of the intersecting surface).
c_{avg}	Average chord of intersecting members (for fuselage intersections, just the chord of the intersecting surface).
$C_{l,int}$	Average section lift coefficient of intersecting members (for fuselage intersections, just the section lift coefficient of the intersecting surface).
Λ_{int}	Average quarter-chord sweep angle of intersecting members in degrees (for fuselage intersections, just the sweep angle of the intersecting surface).
ϕ	Intersection angle
S_{ref}	Reference area

Table 18. Formulas for Hoerner model

Formula	Comments
$C_{d,wall} = \left(0.8\frac{t^3}{c} - 0.0003\right) \frac{c_{avg}^2}{S_{ref}}$	Interference drag coefficient due to wall effect
$C_{d,cl} = 0.1C_{l,int}^2 \frac{c_{avg}^2}{S_{ref}}$	Interference drag coefficient due to lift coefficient effect
$C_{d,sweep} = \left(-0.000018\Lambda_{int}^2 + 0.00009\Lambda_{int}\right) \frac{c_{avg}^2}{S_{ref}}$	Interference drag coefficient due to sweep effect (sweep is in degrees)
$C_{d,inclin} = \left(0.000006\phi^2 + 0.0015\phi\right) \frac{c_{avg}^2}{S_{ref}}$	Interference drag coefficient due to inclination effect (inclination is in degrees)
$C_{d,H} = C_{d,wall} + C_{d,cl} + C_{d,sweep} + C_{d,inclin}$	Total interference drag coefficient for Hoerner model

Tetrault’s CFD model²⁵ is suitable for small thickness ratios less than or equal to 0.075. Similar to the Hoerner model³⁷, this is outside the range of many practical wing-like surfaces and thus necessitates interpolation with Hoerner’s model for intermediate

thickness ratios. Table 19 introduces the variables used in the calculation and Table 20 the relevant formulas.

Table 19. Variables for Tetrault model

Variable Name	Definition
$\frac{t}{c}$	Average thickness ratio of intersecting members (for fuselage intersections, just the thickness ratio of the intersecting surface).
c_{avg}	Average chord of intersecting members (for fuselage intersections, just the chord of the intersecting surface).
ϕ	Intersection angle
S_{ref}	Reference area
Re_c	Reynolds number based on c_{avg}
M_∞	Freestream Mach number

Table 20. Formulas for Tetrault model

Formula	Comments
$C_{d,T} = \left(0.1112 - 0.2572 \sin \phi + 3.44 \frac{t}{c} - 0.02097 \log_{10} Re_c \right. \\ \left. + 0.09009 \sin^2 \phi - 2.549 \frac{t}{c} \sin \phi \right. \\ \left. + 0.0301 \log_{10} Re_c \sin \phi - 0.1462 \frac{t}{c} \log_{10} Re_c \right) \frac{c_{avg}^2}{S_{ref}}$	Interference drag coefficient for Tetrault model
$C_{d,T} = \frac{\sqrt{1 - 0.85^2}}{\sqrt{1 - M_\infty^2}} C_{d,T}$	Compressibility correction

For thickness ratios less than 0.4 and greater than 0.075, a simple interpolation is performed as shown in Equation 13.

$$C_{d,int} = C_{d,T} + (C_{d,H} - C_{d,T}) \frac{\frac{t}{c} - 0.075}{0.4 - 0.075} \quad \text{Eqn. 13}$$

2.1.5 Aerodynamic Methods Validation

2.1.5.1 DLR-F4 Wing-Body Case

The primary aerodynamic subroutines (those containing the methods that, given a subset of an aircraft's geometry and flight conditions, will output the aircraft drag

coefficients) were validated first with an existing model, the DLR-F4 wing-body model (Figure 13).

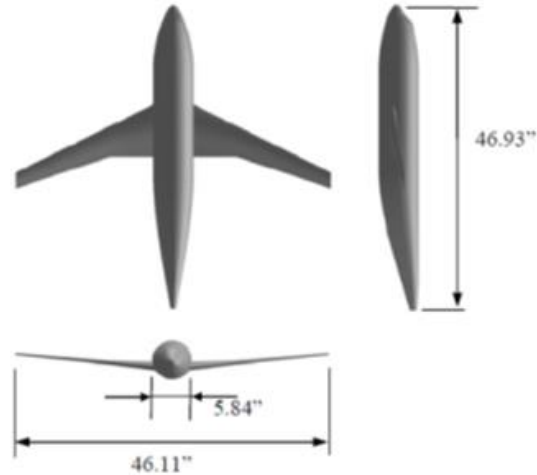


Figure 13. DLR-F4 wing body model⁸

This model has been validated in the VT MDO code in the past⁸ with experimental wind-tunnel data and CFD results and was chosen here due to its simplicity. Fuselage cross-section is nearly circular, a shape that could be modeled in both the VT MDO and PACELAB-VT parameterization schemes. This simplicity also allowed the validation process to focus on the mathematical correctness of the codes written for PACELAB-VT over the course of the study, and they were tested for each drag component individually. To compare with wind tunnel results, a Mach number point of 0.8, a lift coefficient of 0.7 and a relative freestream Reynolds number of $6.54E6 \text{ ft}^{-1}$ were utilized as the freestream conditions. Recall that profile drag is not a function of lift coefficient. Results are summed up in Table 21.

Table 21. DLR-F4 code comparison results (Mach 0.8, Relative Re 6.54E6 ft⁻¹, Lift Coefficient 0.7). VT MDO code vs. PACELAB-VT.

Drag component	% Difference	Difference in drag counts
Cd_profile	+0.02	+0.03
Cd_interference	+5.3	+0.54
Cd_wave	+2.03	+3.3

Very small differences in the profile drag can be explained by the difference in parameterization used by the VT MDO code and that added in PACELAB-VT. The VT MDO code starts the wing panels at a point slightly past the root, while the new code implemented in PACELAB-VT begins them immediately at the root. This results in slightly different wetted areas that are calculated.

The larger differences in wave and interference drag are explained by the fact that the new work done in PACELAB-VT assumes an exact analytic elliptic distribution. The Trefftz plane analysis used for the induced drag in the VT MDO code will ‘find’ the distribution that gives the minimum induced drag for a given configuration. For a single lifting surface, as in the DLR-F4 model, this will be an elliptical distribution. For multi-surface vehicles the situation is more complicated. As two lifting surfaces approach each other in the y-z plane (that is, looking head on to the vehicle), the minimum induced drag results in the sum of the individual distributions approaching the elliptical case, not necessarily the individual distributions. As the surfaces gain vertical offset from each other, their individual distributions tend toward elliptical. This will have a noticeable effect in the validation case run with a Boeing 737-800 like aircraft, in the following section. It does not affect the DLR-F4 case, which has a single lifting surface, therefore a minimum-drag distribution that is elliptical should result. However, because this is a numerical method it does not follow the elliptical case perfectly, as can be seen in Figure

14. This affects both wave and interference drag. Inclination angle (discussed in Section 2.1.4) is also approximated for the fuselage cross-section point-list, which deviates from the VT MDO code's smooth cross-sections.

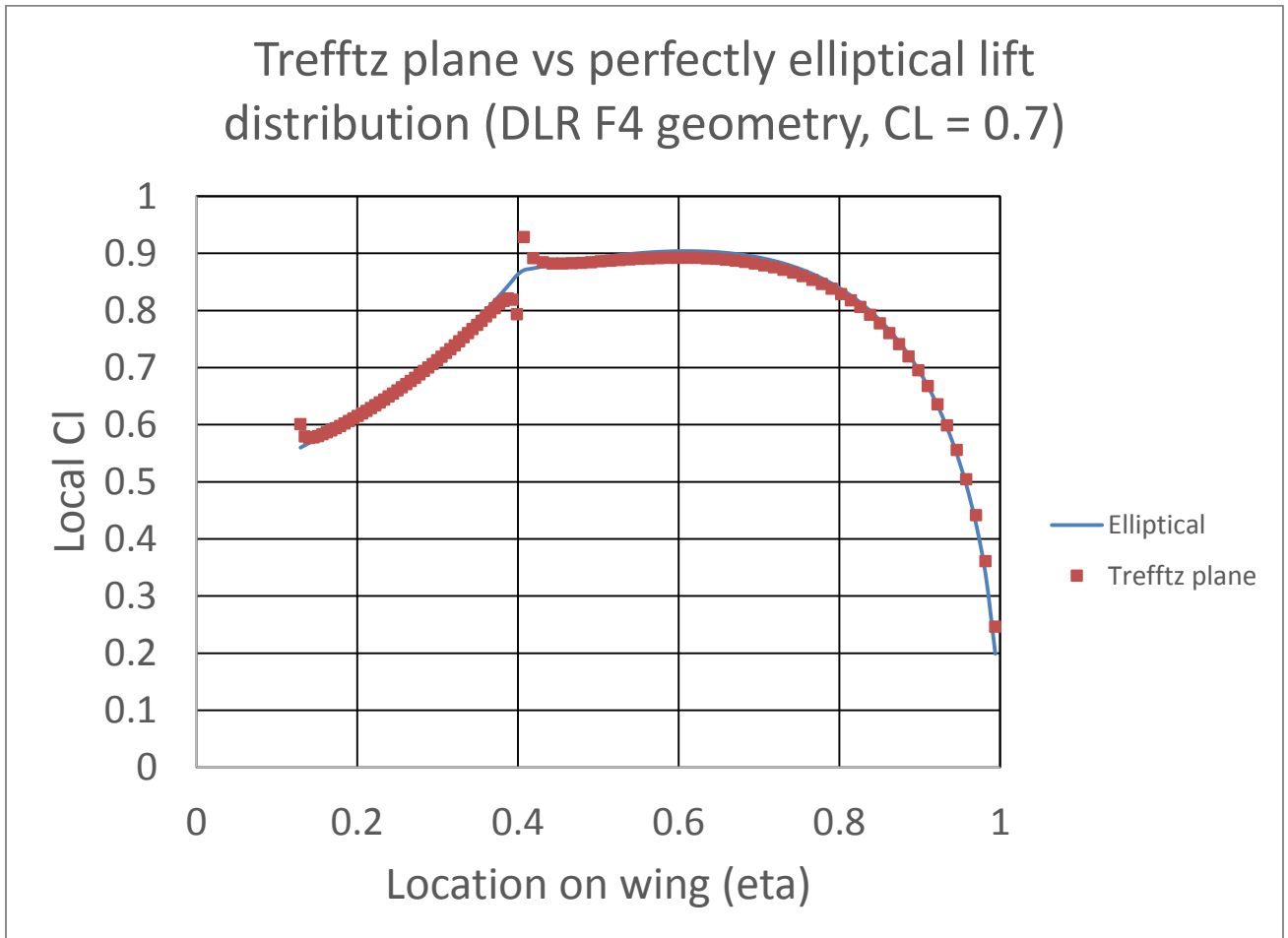


Figure 14. Elliptical distribution vs. VT MDO Trefftz plane method, DLR-F4 wing

Figure 15 showcases the drag buildup alongside wind tunnel data (note the induced drag from the VT MDO code, which was not added to PACELAB APD 3.1 during the course of this study, is shown on the right of the graph). Also shown is the PACELAB APD 3.1 / PACELAB-VT induced drag for the DLR-F4. The VT MDO induced drag at low to middle range lift coefficient values shows good agreement, while

the PACELAB induced drag shows good agreement at high lift coefficient values.

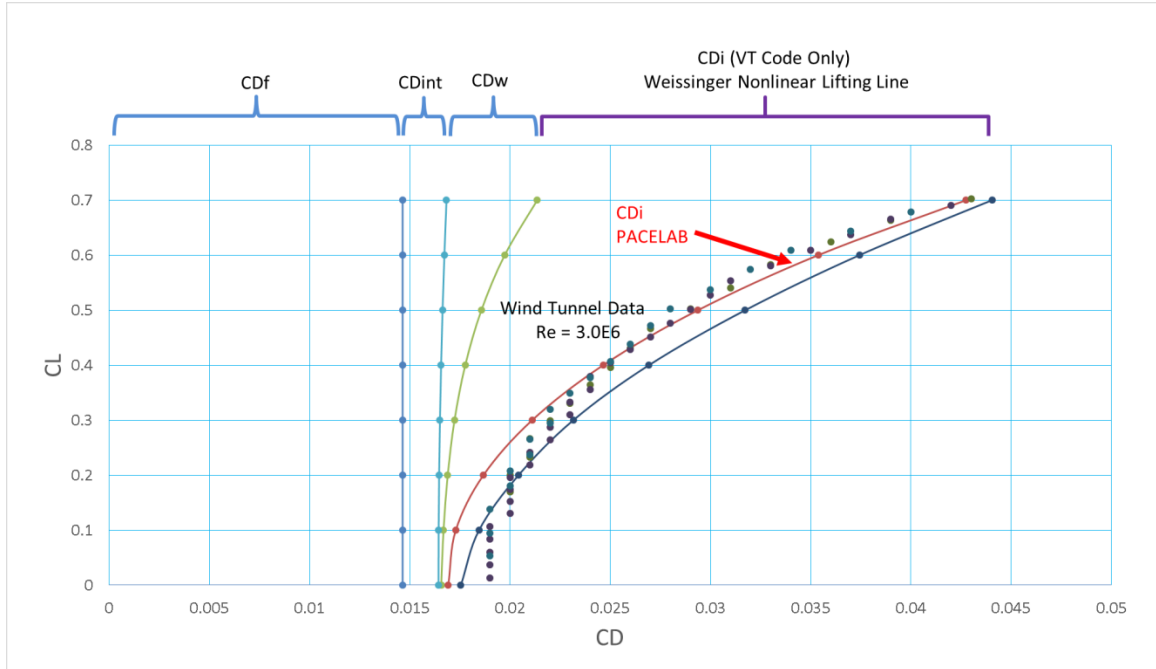


Figure 15. DLR-F4 drag polar predicted with PACELAB-VT (Mach 0.75, Relative Reynolds Number $3.0E6 \text{ ft}^{-1}$)

2.1.5.2 737-800 Case

A second validation case, a 737-800 model was also selected, to test additional geometry-processing code structures added in PACELAB-VT as well as to validate the method for a full configuration (Figure 16). An existing model of a B737-800 model in the VT MDO code was used as a comparison against the 737-800 model in PACELAB-VT.

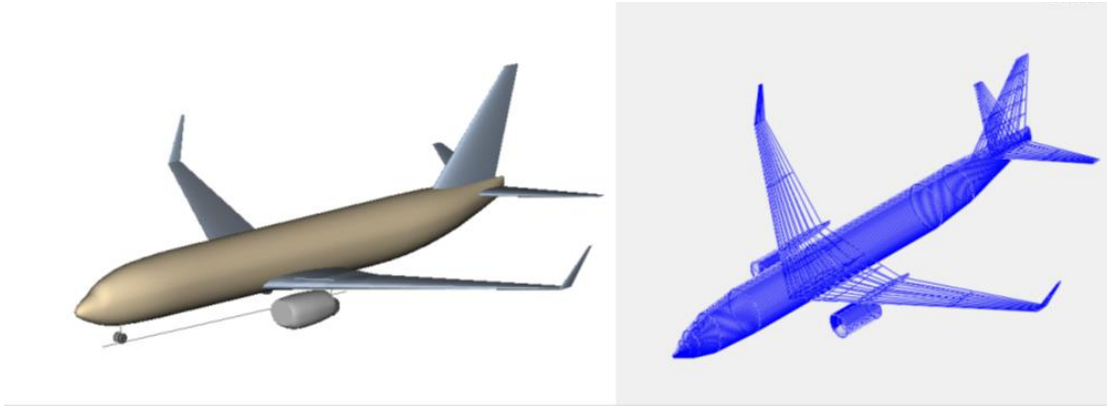


Figure 16. Pacelab 737-800 model (left) and VT MDO model (right)

Some small geometric modifications were made to both models in an attempt to bring them as close together as possible:

- Forced constant leading edge sweep in VT MDO model to match PACELAB-VT leading edge sweep, as PACELAB-VT does not allow for variable leading edge sweep
- Fuselage and nacelle length / maximum diameter in PACELAB-VT model edited to match VT MDO model
- Wing / winglet geometric parameters in PACELAB-VT model (root / kink locations, span, sweep angles, dihedral, chord lengths, thickness ratios) edited to match VT MDO model
- Stabilizer geometric parameters in PACELAB-VT model (root location, span, sweep angles, dihedral, chord lengths, thickness ratios) edited to match VT MDO model
- Fin geometric parameters in PACELAB-VT model (root location, span, sweep angles, chord lengths, thickness ratios) edited to match VT MDO model

- C.G. location in VT MDO model (for trimmed aircraft calculations)
imported from PACELAB-VT model

This affects the wetted area calculation for the wing and tail (profile and wave drag), form factor calculations (profile drag), as well as inclination angle calculations for interference drag. Wing / empennage geometry was able to be forced to a nearly identical state between the two models, but the completely different fuselage cross-section parameterizations introduced a small degree of difference in wetted area and inclination angle calculations.

Generated drag polars are shown in Figures 17-19 for three Mach-altitude combinations approximating cruise conditions. The results from the VT MDO code are shown alongside those from this study (VT MDO methods for wave, interference and profile drag, with the PACELAB APD 3.1 induced drag component). As third and fourth comparisons the default PACELAB APD 3.1 and FLOPS drag calculation for all components are also shown.

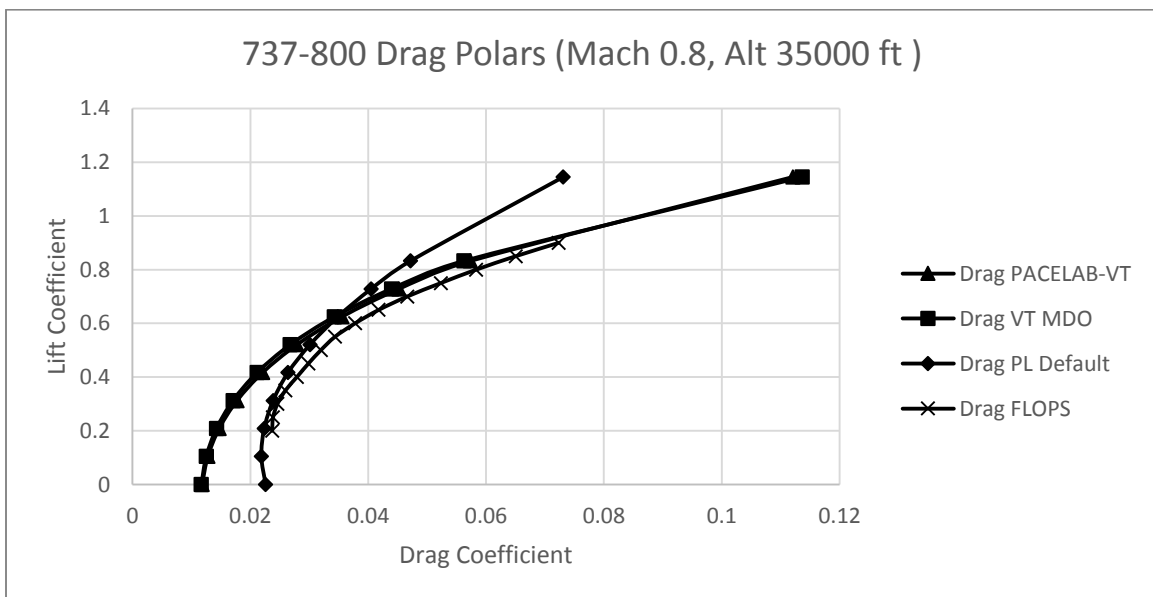


Figure 17. 737-800 drag polar (Mach 0.8, Alt 35000 ft)

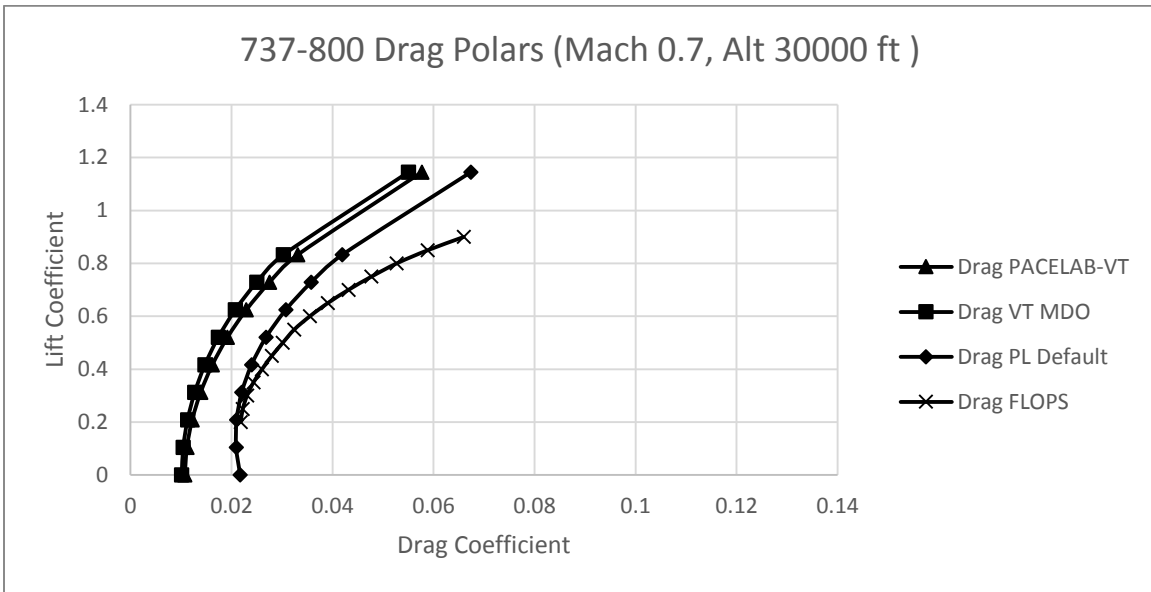


Figure 18. 737-800 drag polar (Mach 0.7, Alt 30000 ft)

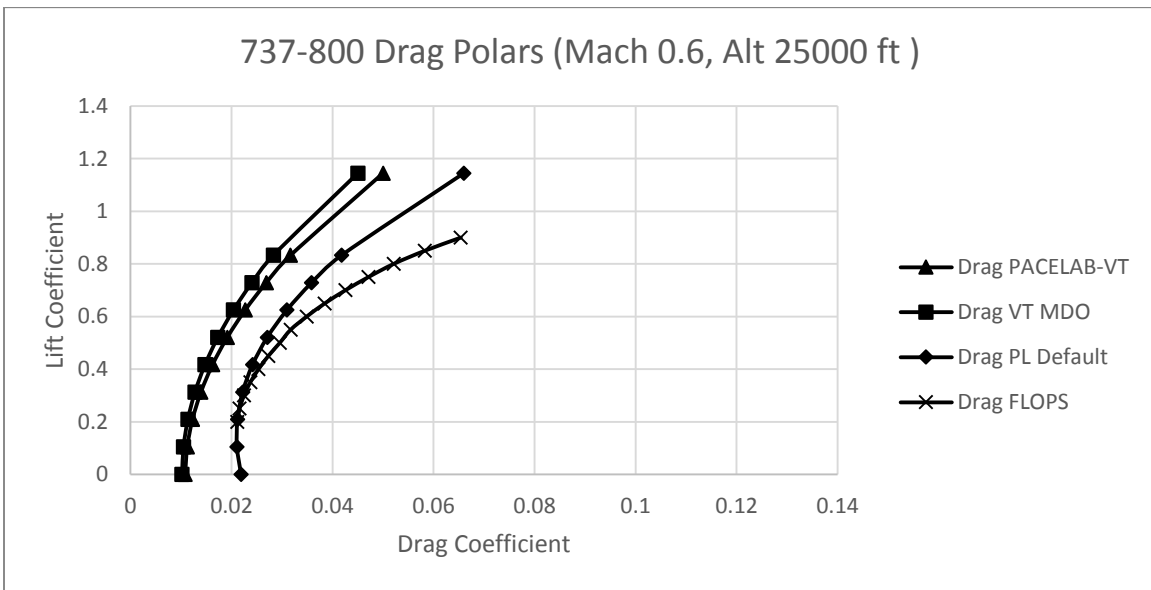


Figure 19. 737-800 drag polar (Mach 0.6, Alt 25000 ft)

As can be seen from the curves, there is a considerable difference between PACELAB APD 3.1 drag calculations and the new method predictions, which is to be expected because the PACELAB APD 3.1 methods are empirically based and

substantially different from the new methods³⁶. PACELAB methods assume transition very close to the leading edge, whereas PACELAB-VT and VT MDO calculate values of transition that can range from 10-70% of the relative chord length (recall the discussion in Section 2.1.2.1). Referring back to Figure 15 and the corresponding wind tunnel data, it would seem that at a transonic Mach number appropriate for cruise the PACELAB-VT curves are closest to physical reality for lift coefficients in the cruise regime ($CL = 0.4-0.6$). It can also be seen that the VT MDO and PACELAB-VT drag predictions diverge at higher lift coefficients, and lower Mach numbers. This is due to differences in both wave drag (because of the differences in lift distributions from the Trefftz plane analysis and the exact elliptical assumption in this study) and induced drag. Individual component differences are examined in detail below. It can also be seen in the figures that the FLOPS drag predictions are consistently higher, due to an earlier onset of drag rise (discussed further in Section 3.1) at lower Mach numbers.

Figures 20 and 21 show the differences between the VT MDO and PACELAB-VT total drag coefficient in both relative (percent) and absolute (drag count) considerations. These and all following figures here pertain to the ‘modified’ models that were geometrically modified to match each other as closely as possible. Note the increase in difference with decrease in Mach number. This is due primarily to differences in wave and induced drag. These differences will be explored in further detail next.

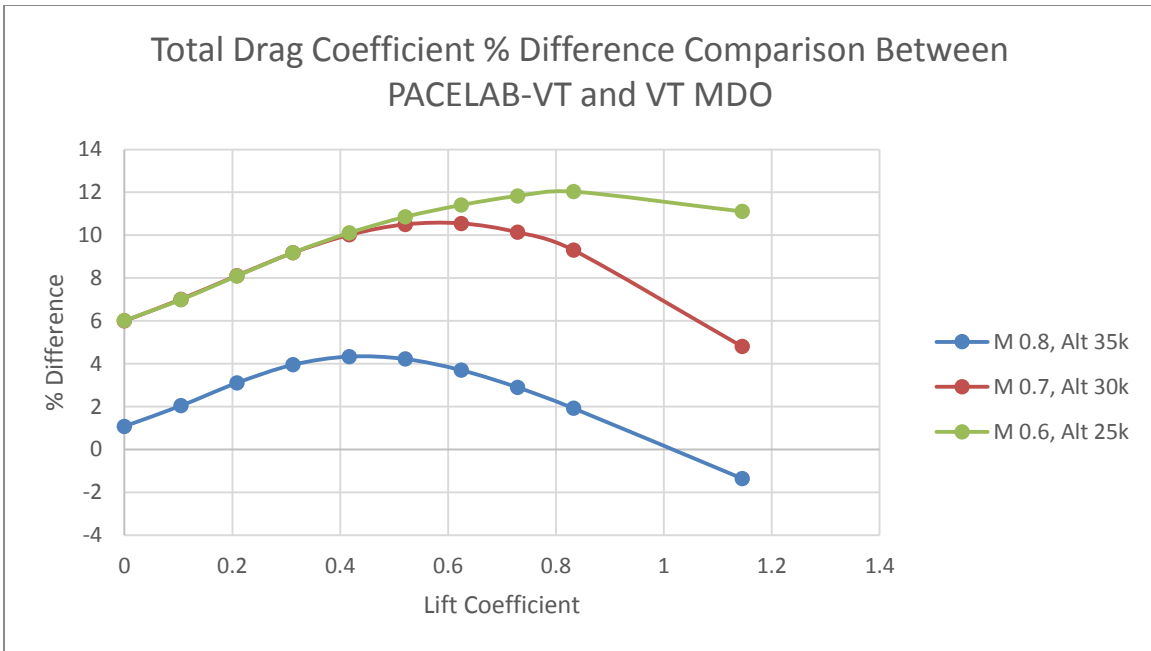


Figure 20. Total drag coefficient % difference comparison (737-800)

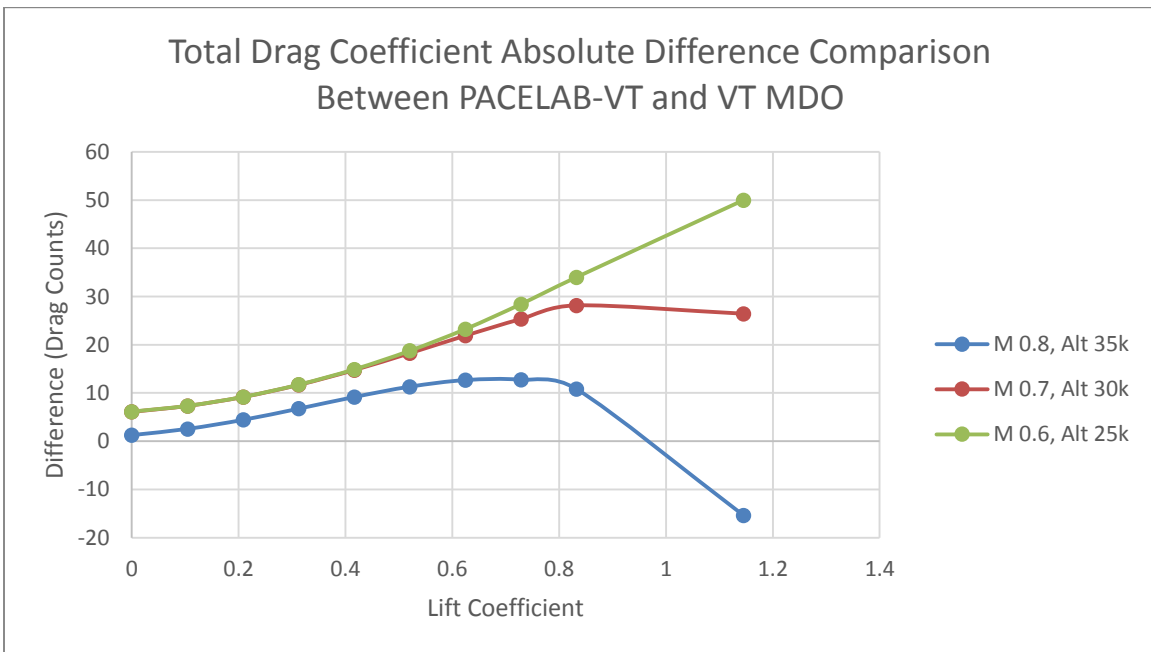


Figure 21. Total drag coefficient drag count difference comparison (737-800)

The validity of assuming an elliptical distribution (for the calculation of wave and interference drag) with the default induced drag calculation in PACELAB APD 3.1 was also tested. Recall that PACELAB-VT does not directly calculate a lift distribution, but

only the span efficiency, using the default method from PACELAB APD 3.1. Induced drag coefficients for both the wing and stabilizer in PACELAB APD 3.1 / PACELAB-VT are calculated from:

$$C_{D,i} = (1 + \delta) \frac{C_L^2}{\pi AR} \quad \text{Eqn. 17}$$

δ is estimated from wing taper ratio and is zero for the elliptic case. Therefore, to quantify the difference between the elliptic assumption used in this study, and the actual distribution indirectly assumed by PACELAB APD 3.1 / PACELAB-VT, two cases were considered:

- Calculated δ (method from Torenbeek⁶)
- ‘Forced’ $\delta = 0$ (elliptic)

The difference in the wing induced drag between the two cases, for a given flight condition, gives a rough estimate of how close the elliptic assumption is to the lift distribution indirectly assumed by PACELAB APD 3.1 / PACELAB-VT. Figure 22 shows these differences. Recall from Section 2.1.1 that the tail is assumed to have a 2% increase in tail induced drag coefficient from the elliptic case. Tail induced drag is small compared to wing induced drag, so the effect of this on the overall induced drag coefficient is minimal.

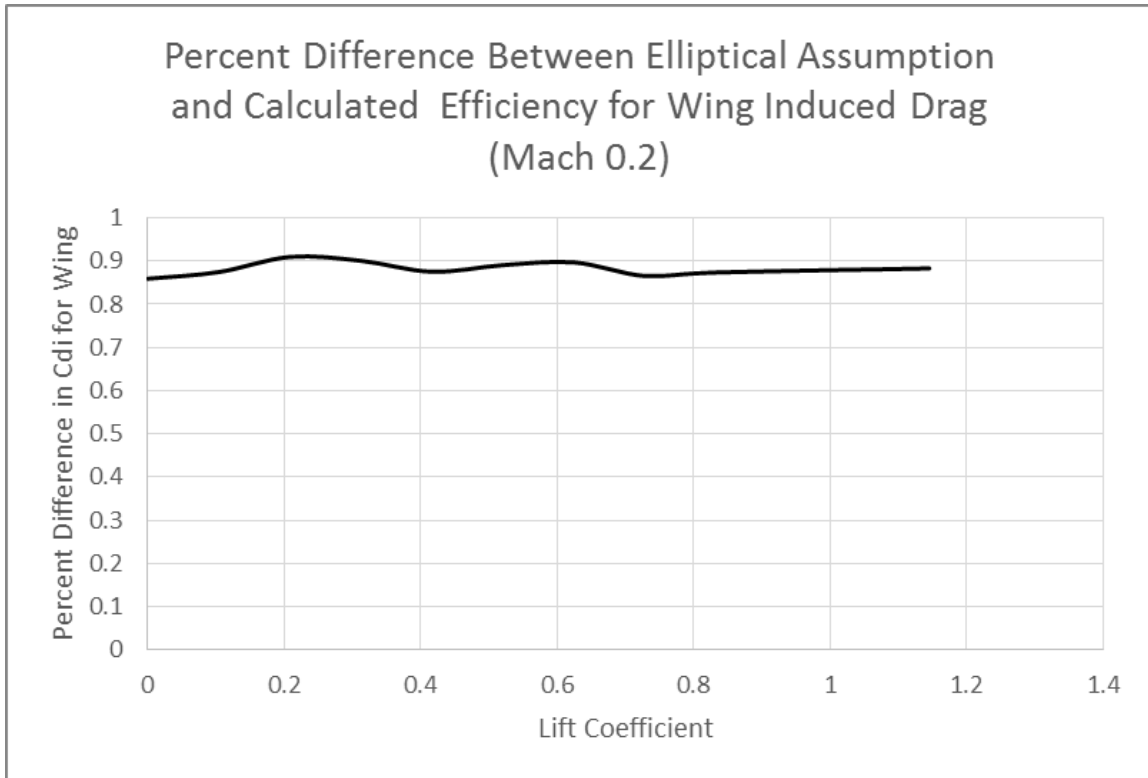


Figure 22. Elliptical and calculated efficiency comparison (Mach 0.2, 747-800)

This shows that the assumption of an exact elliptical distribution, for the calculation of wave and interference drag, is close to the distribution that would produce the estimated efficiency that PACELAB-VT calculates from the empirical methods in Torenbeek⁶. There are additional differences in the induced drag, however (in the form of a contribution from the fuselage), that will be discussed later.

Figures 23 and 24 show the relative and absolute differences for the profile drag for the three different Mach-altitude points chosen. Recall that profile drag is not a function of lift coefficient. As can be seen from the figures, both relative and absolute differences are low, less than 5% and 5 drag counts, respectively. This difference is due to small differences in strip wetted area calculations, because of the different fuselage cross-sectional shapes. Because PACELAB-VT and the VT MDO do not use the same

fuselage parameterizations, the fuselage cross-sections do not match each other exactly; they differ by enough to cause the wetted areas of the wing and tail to differ by roughly 5%. The output was examined line by line and it was found that each strip in PACELAB-VT differed from its counterpart in the VT MDO code by about 5%, all across the wing and tail. This was verified to be the source of the difference by running a case where the wetted areas in PACELAB-VT were ‘forced’ to equal their values in the VT MDO code, and the difference in profile drag coefficient dropped to less than 0.1%, confirming the wetted area calculation as the source of the difference. Any residual difference remaining would be a result of slight differences in atmospheric models (used in calculating Reynolds numbers) as this is the only other potential source of differences.

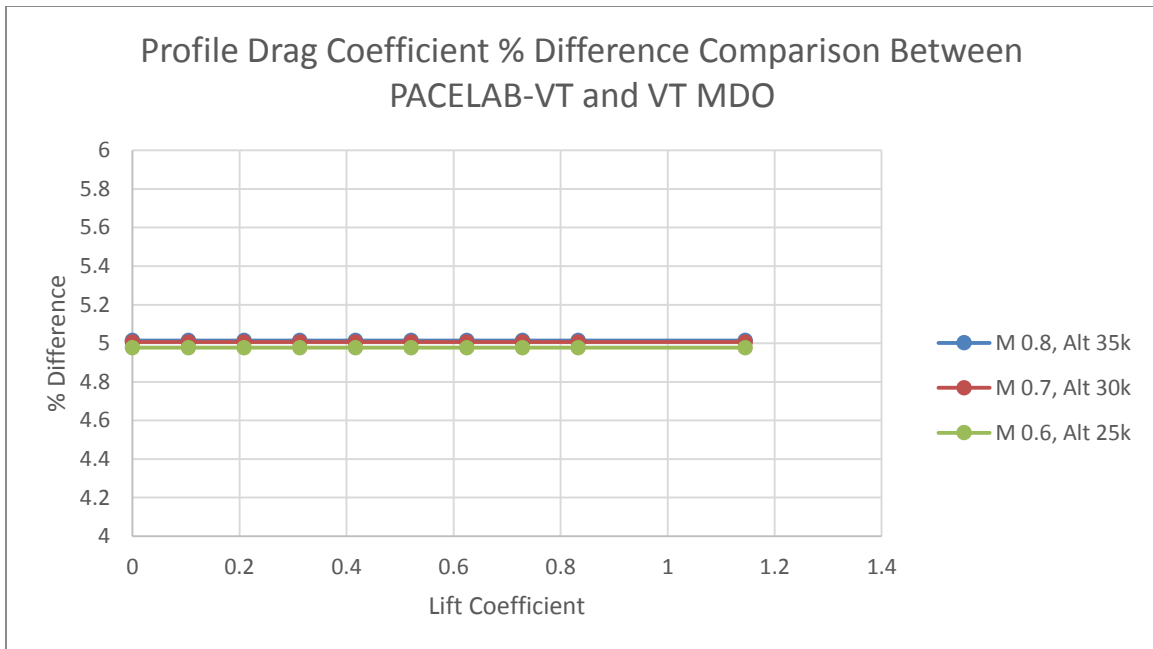


Figure 23. Profile drag coefficient % difference comparison (737-800)

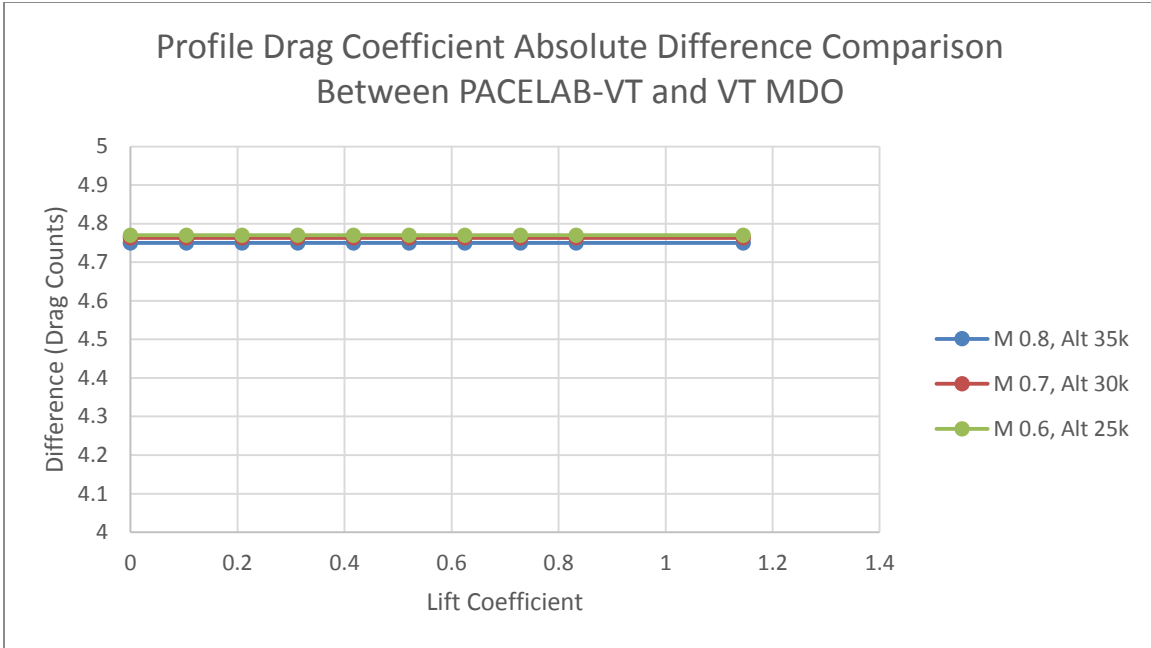


Figure 24. Profile drag coefficient drag count difference comparison (737-800)

For all test cases, the interference drag coefficient was of very low magnitude compared to other drag components (on the order of $10E-4$). Figures 25 and 26 show the relative and absolute differences in interference drag between PACELAB-VT and the VT MDO method. As can be seen from the curves, both relative and absolute differences are quite small, although they do increase with lift coefficient. This is due to the difference in section lift coefficient at the intersection, an issue which will also be encountered again with larger consequences in the wave drag coefficient calculation below.

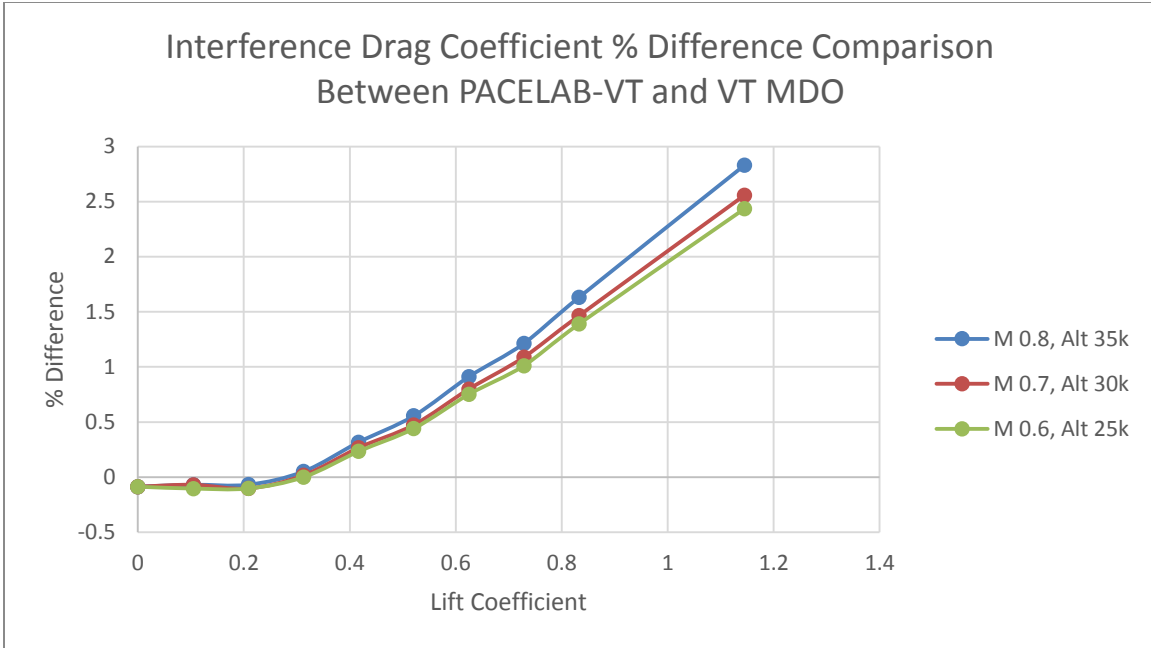


Figure 25. Interference drag coefficient % difference comparison (737-800)

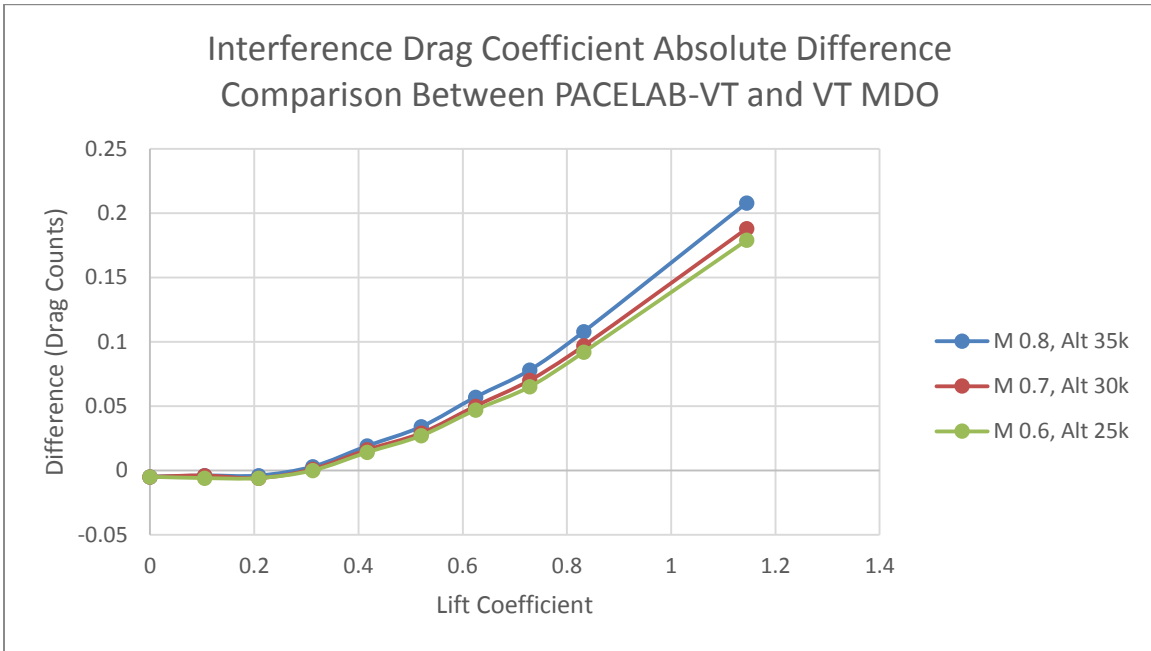


Figure 26. Interference drag coefficient drag count difference comparison (737-800)

A case was run ‘forcing’ the section lift coefficient at the intersection to the VT MDO value, and the differences became negligible, further supporting the conclusion that

residual differences are due to the small difference in the lift distributions at the root locations.

The effects of differences in lift distributions between the Trefftz plane analysis (VT MDO) and the exact elliptical distributions assumed in this study are most apparent in the wave drag coefficient calculation. Figures 27 and 28 show the relative and absolute differences in wave drag coefficient for the three Mach-altitude points chosen for the validation.

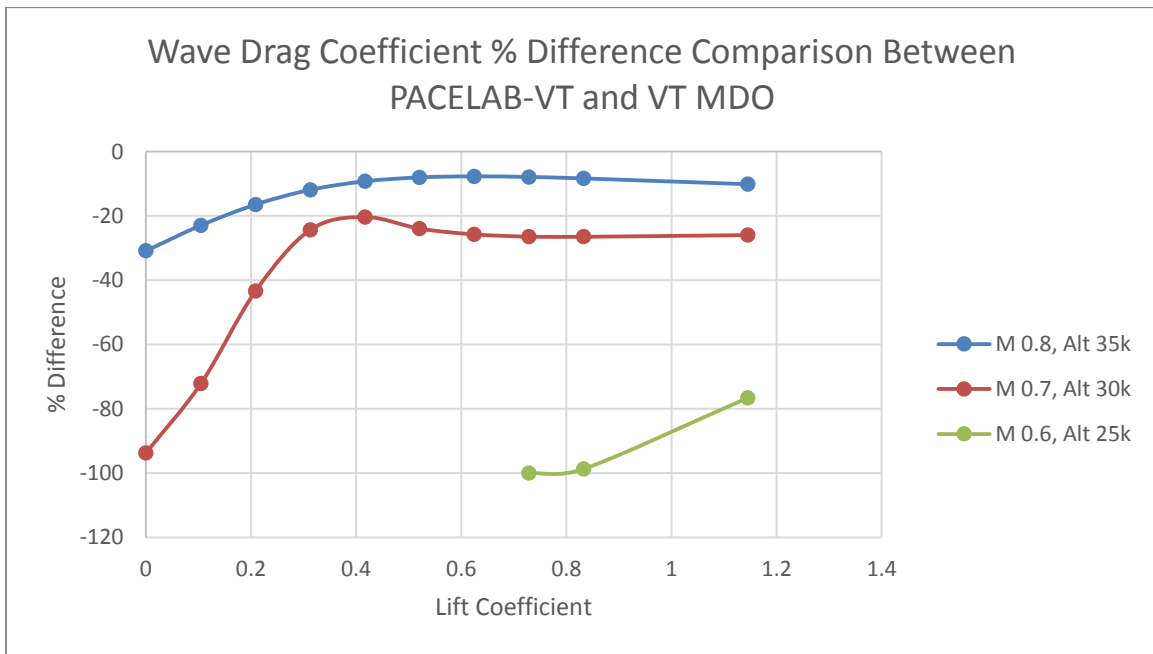


Figure 27. Wave drag coefficient % difference comparison (737-800)

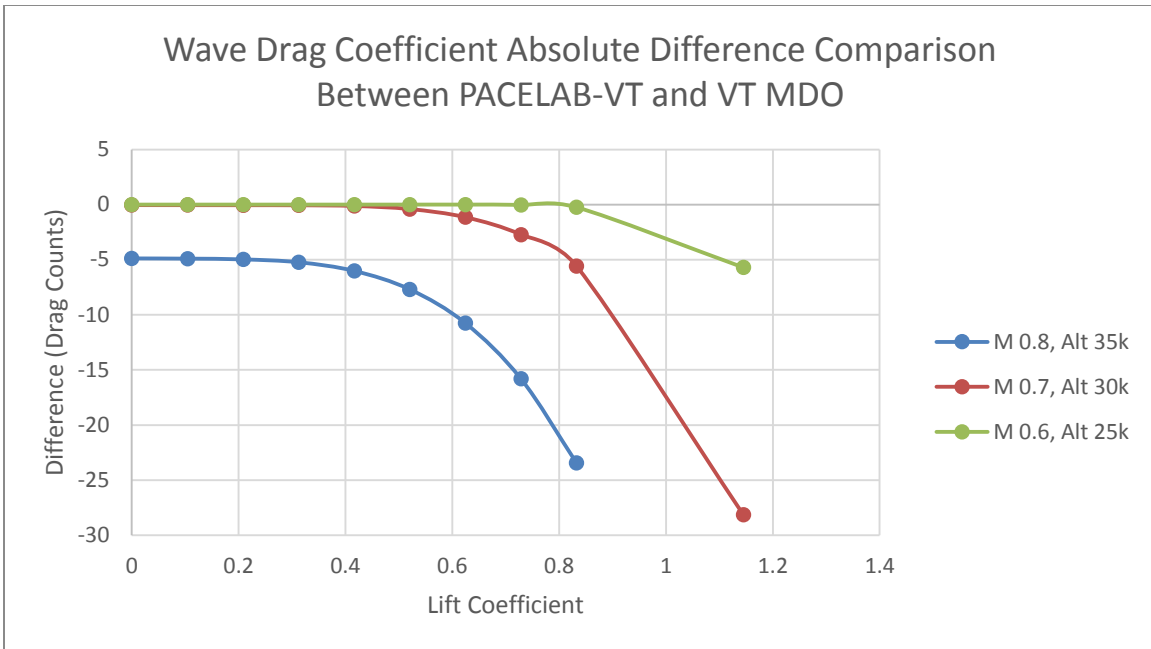


Figure 28. Wave drag coefficient drag count difference comparison (737-800)

Key points to note from these figures include the inverse relationship between the relative and absolute differences. Similar to the differences in the induced drag, this is because at low lift coefficients the wave drag coefficient is very small, and the relative differences increase because of this while the absolute differences decrease. At higher lift coefficients (CL greater than 0.4) the absolute difference rapidly begins to increase (Figure 28), a phenomenon which will be explored in further detail here. First it should be stated that to confirm that the lift distribution was the source of the differences seen here, a case was run in which the section lift coefficients along the wing were ‘forced’ to the corresponding VT MDO values, and the final difference in wave drag coefficient became negligible.

Looking at a sample of the output from both the VT MDO and PACELAB-VT codes, it is possible to reconstruct and compare the lift distributions. Figures 29 and 30 show the lift distribution (and section lift coefficient distribution) across the 737-800

wing at a lift coefficient of $CL = 0.8$. Note the ‘noise’ in the numerical method at kink location and winglet root location, similar to what can be seen for the DLR-F4 case in Figure 14. However, the elliptical case is not as close a fit for the 737-800 as it was for the DLR-F4. This is because of the effect of multiple lifting surfaces on the VT MDO Trefftz analysis, as discussed in Section 2.1.1. Two lifting surfaces in close proximity in the y-z plane will cause the distribution for minimum induced drag, in the Trefftz plane analysis, to drive the *sum* of the individual distributions toward the elliptical case. As the surfaces move further apart their individual distributions will tend toward elliptic for minimum total induced drag. For cases such as the 737-800 model here, its effect on the differences in distribution and on the overall wave drag calculation is significant.

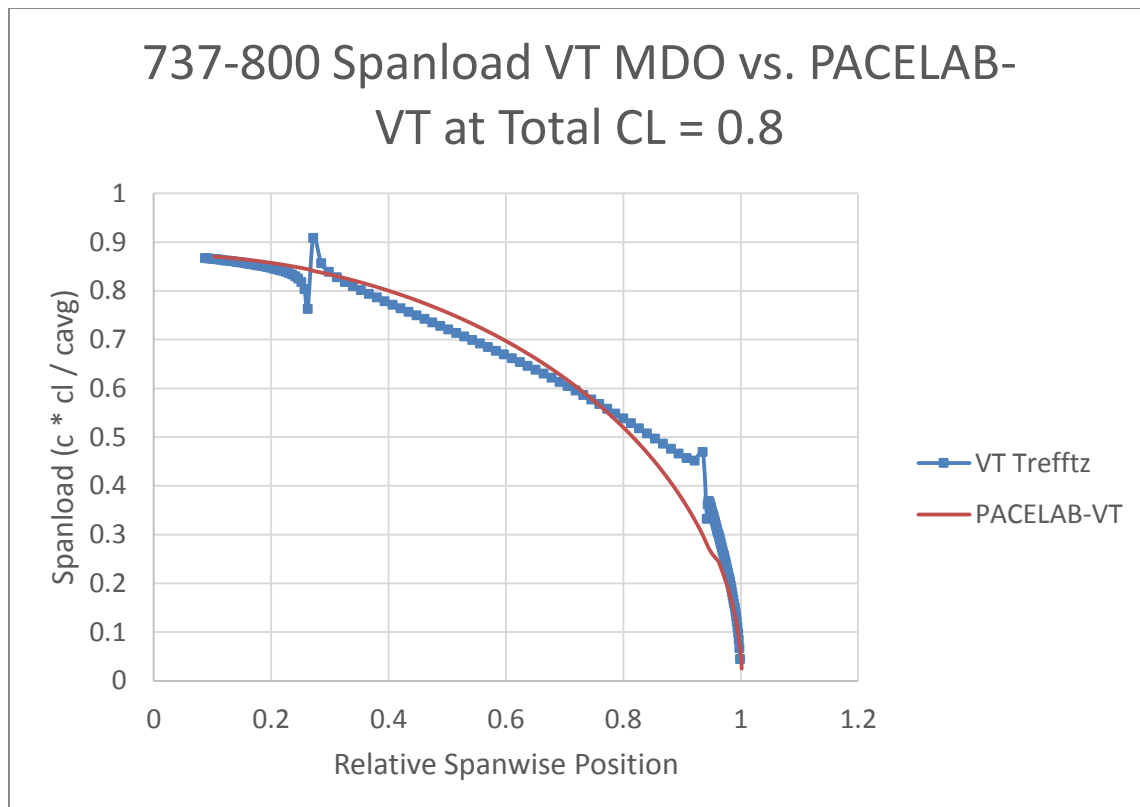


Figure 29. 737-800 wing lift distribution comparison between Trefftz plane and elliptical

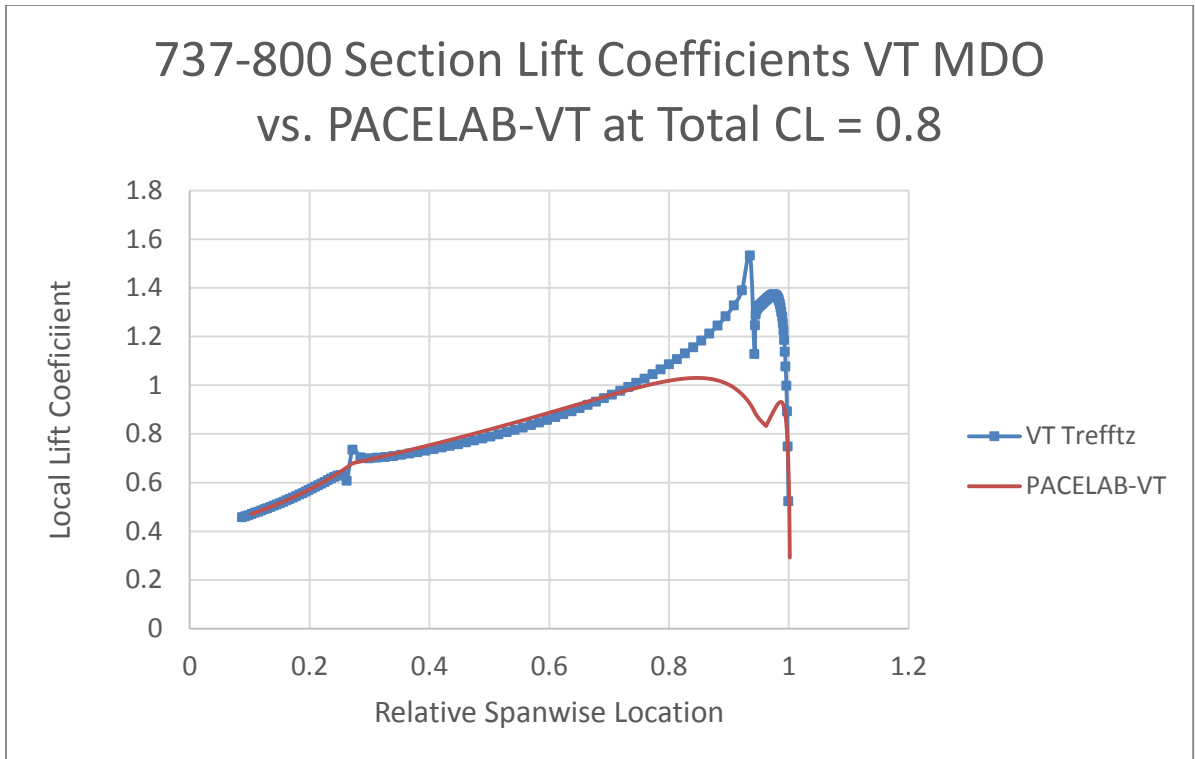


Figure 30. 737-800 wing section lift coefficient comparison between Trefftz plane and elliptical

This effect on the calculation process is shown in Figures 31-33. Figure 31 shows the relative (percent) differences between section lift coefficients of the VT MDO and PACELAB-VT code models across the wing. Carrying the process through to the calculation of critical Mach number (Figure 32), the relative differences do not change by large amounts. However, the final step of the process, calculation of wave drag coefficient from critical Mach (Locke’s 4th Power Law) increases the relative difference by more than a factor of 2 at most spanwise locations.

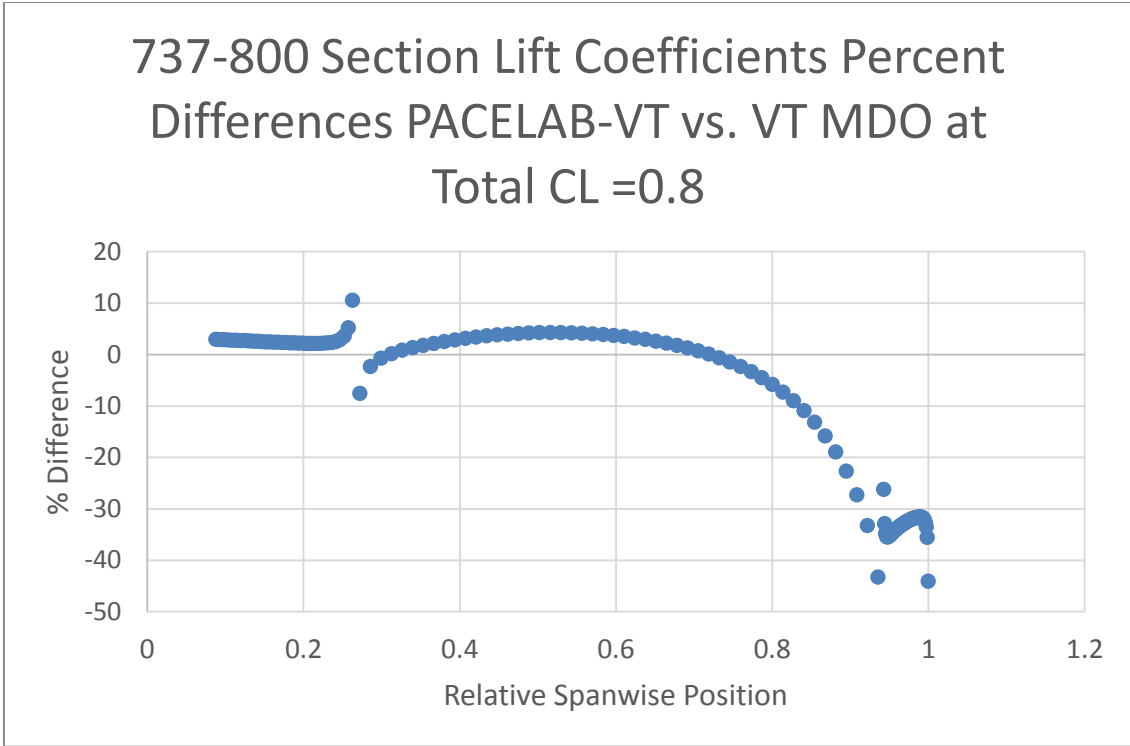


Figure 31. 737-800 relative difference in section Cl across wing (CL = 0.8)

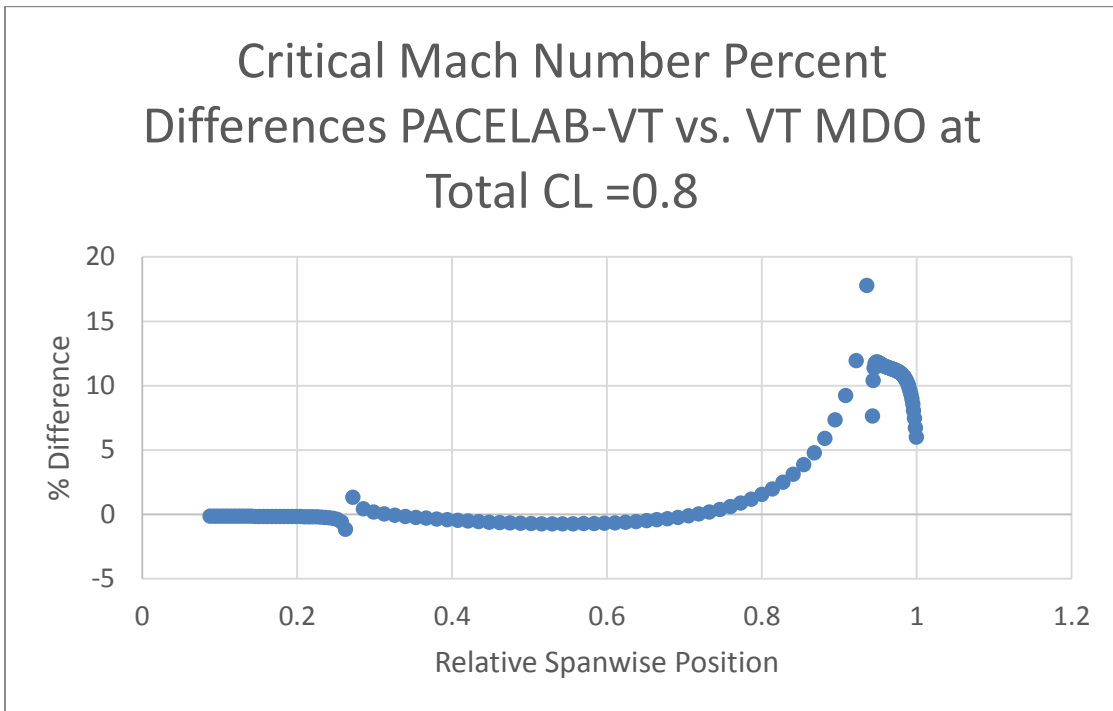


Figure 32. 737-800 relative difference in critical Mach across wing (CL = 0.8)

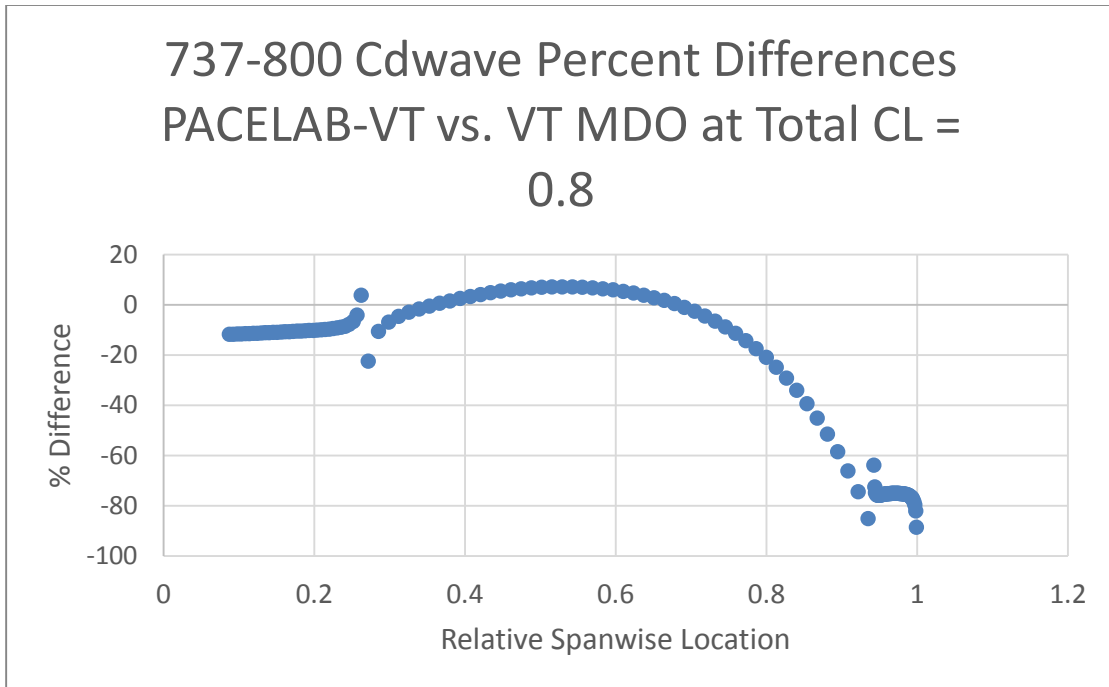


Figure 33. 737-800 relative difference in Cd_w across wing (CL = 0.8)

The induced drag sees noticeable differences observed in the drag calculation for the 737-800 model as shown in Figures 34 and 35.

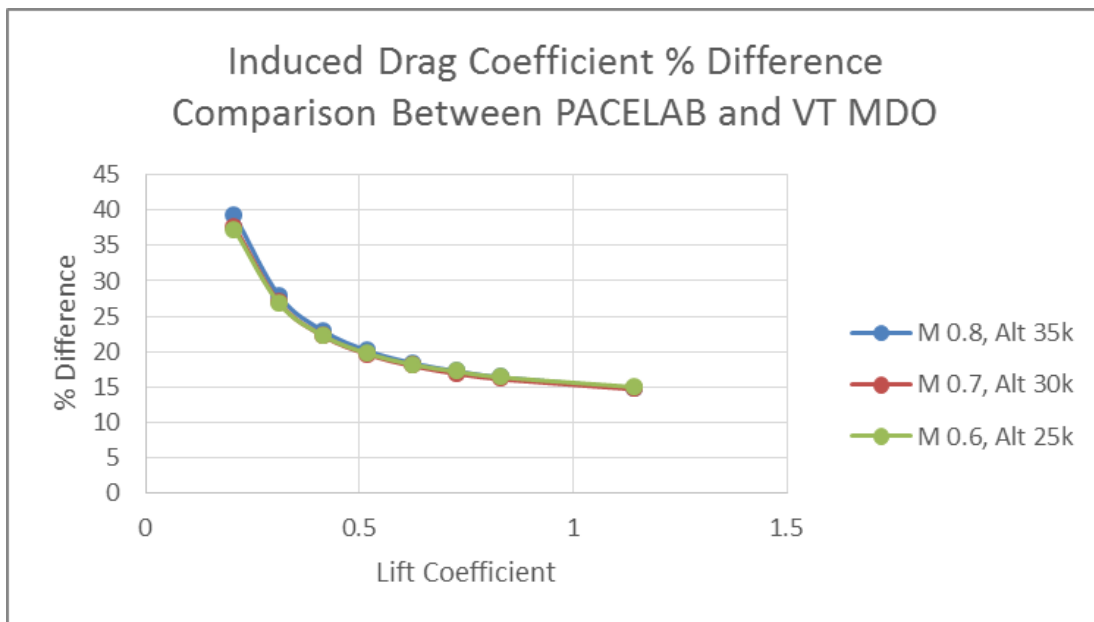


Figure 34. Induced drag coefficient % difference comparison (737-800)

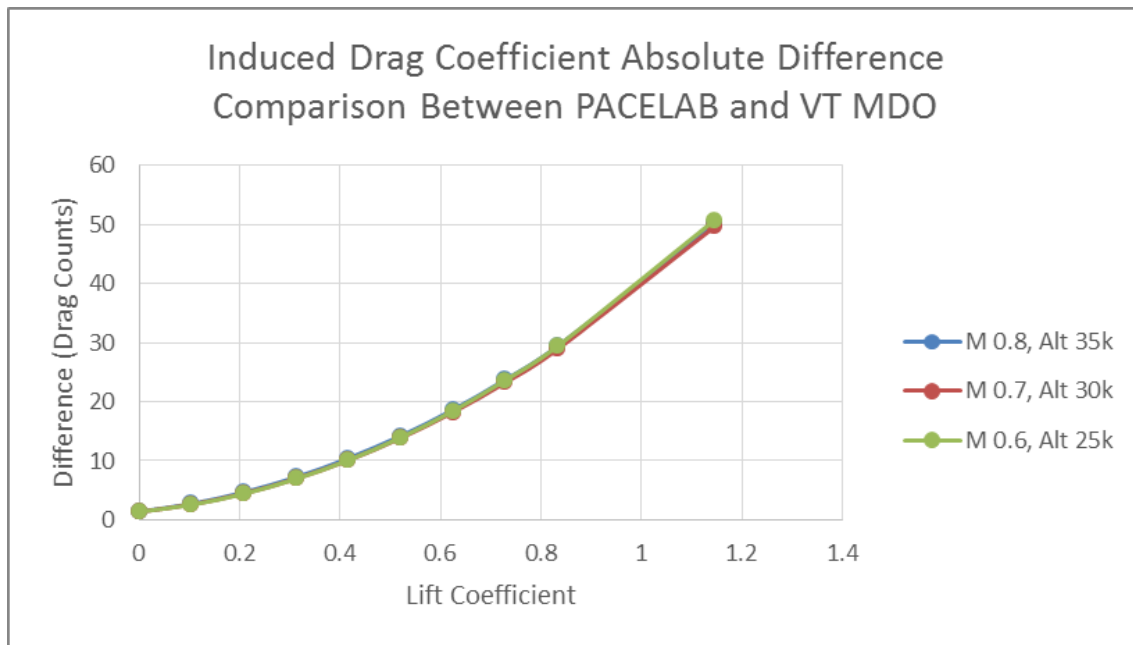


Figure 35. Induced drag coefficient drag count difference comparison (737-800)

Note that this is a comparison between PACELAB APD 3.1 / PACELAB-VT induced drag and the VT MDO code, as the VT MDO induced drag was not part of the work plan in this study.

As can be seen in the figures, there is a general increase in the absolute differences with lift coefficient. As lift coefficient increases, so does induced drag, so this makes sense. It can also be seen that there are very high relative differences at low lift coefficients. This is because as the values of induced drag get smaller (smaller lift coefficient) their relative differences increase even though the absolute difference shrinks. It is expected that there will be significant differences between the induced drag values. PACELAB uses semi-empirical methods developed in Torenbeek⁶ and Raymer¹, and in the transonic regime ‘interpolates’ between a subsonic and supersonic method³⁶. Unlike the VT MDO method, this results in induced drag being a function of Mach number as well as lift coefficient. Another important difference is that PACELAB does not calculate the effect of a winglet

on the induced drag. It requires the user to select a calibration increment (in the form of a percent-reduction in wing induced drag coefficient) for the presence of a winglet. For the purpose of this validation, a value for this increment was chosen based on running two cases of the 787-800 model in the VT induced drag code (which takes into account the winglet), one with winglets and another without. Based on analysing the percent-differences in induced drag coefficient a fixed value of -21.8% was utilized for the winglet calibration increment in PACELAB-VT. This brought down significantly the induced drag calculated by PACELAB-VT, bringing it closer to the VT MDO calculated value.

The PACELAB-VT method also includes an estimation of fuselage induced drag, which additionally impacts the differences between the VT MDO and PACELAB-VT methods. Figures 36 and 37 show the relative and absolute effects of the fuselage drag on the overall induced drag coefficient in PACELAB-VT at a low Mach number, out of range of the effects of interpolating between the subsonic and supersonic induced drag methods. The ‘with-fuselage’ (blue) curves are virtually identical to those in Figures 36 and 37. The change in difference due to fuselage effects is significant enough that it effectively doubles the differences between the VT MDO and PACELAB-VT induced drag methods for the overall induced drag coefficient at lift coefficient values greater than 0.4.

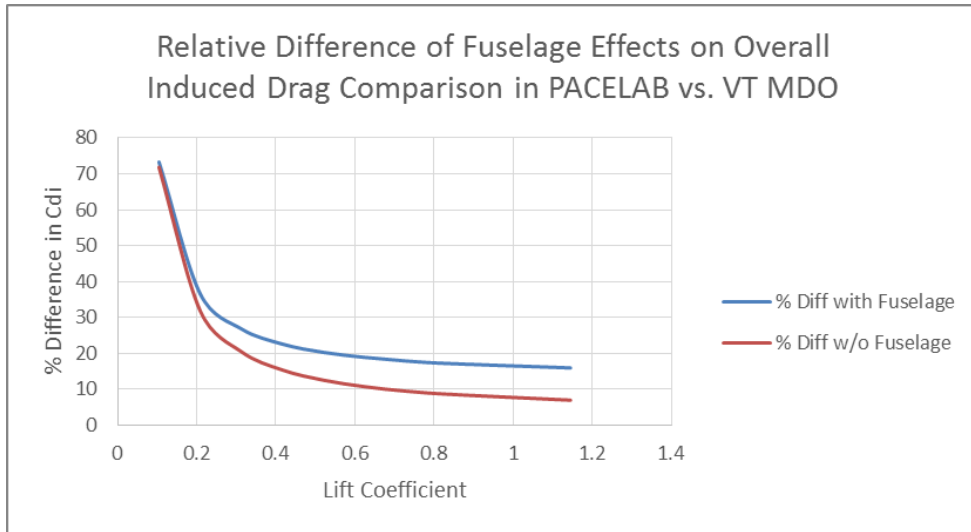


Figure 36. Fuselage relative effects on induced drag coefficient comparison (Mach 0.2, 737-800)

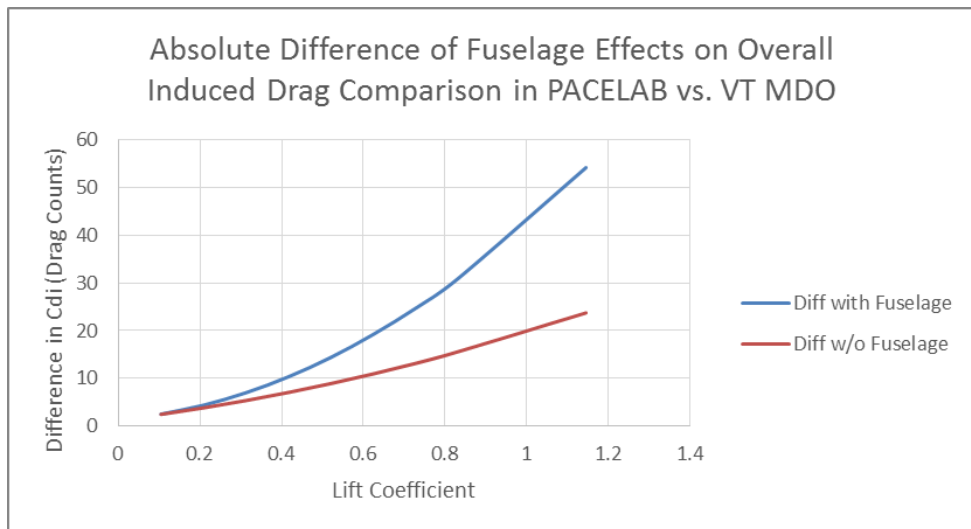


Figure 37. Fuselage absolute effects on induced drag coefficient comparison (Mach 0.2, 737-800)

2.2 Strut-Braced Wing Cases

Verification that the strut itself had been correctly parameterized (that is, the user-set geometry was working correctly) was carried out through simple physical representation. Three-views of the strut component on the aircraft were generated and

printed out, and with the aid of a ruler and protractor it was verified that all relative positions, distances, lengths, angles, etc. were correct.

To verify that the drag calculation was working correctly, the 737-800 model utilized in the aerodynamic validation was modified to allow for the presence of a strut, including raising the wing to the top of the fuselage (high wing configuration). Because only the strut was a concern for validation, other portions of the aircraft geometry such as tail dimensions were left unchanged. A corresponding model was selected from the VT MDO library to verify that the strut drag updates were working correctly. It was deemed that as long as the struts matched between the two models, other aircraft parameters (that did not affect strut drag estimation) were inconsequential. The fuselage cross-sections were similar enough that differences in geometry were negligible (inclination angle and wetted area calculation).

Similar to the previous aerodynamic validation, three representative Mach altitude points were chosen and the corresponding drag output of the strut was measured for all three in both the PACELAB-VT work and the VT MDO code.

Due to the elimination of lift coefficient as a contributing factor, and the fact that only a single component was being considered, all values for interference and profile drag were very close (<1% difference) through the range of Mach-altitudes chosen. Wave drag was off by 6%, which initially seems worrisome but is due to the extreme sensitivity of Locke's 4th Power Law to differences in drag divergence Mach number (see the wave drag discussion in Section 2.1.5.2). Here a difference of less than 1% in M_{DD} results in a six percent difference in total wave drag coefficient. However, this 'relative' difference is misleading as the number is so small that the absolute difference was less than a fifth of a

drag count. Recalling the discussion from earlier, as relative differences go up (that is, as the coefficients get smaller) the absolute differences go down. Finally, induced drag for the non-lifting strut case is of course zero.

2.3 Other Models Implemented in PACELAB-VT

2.3.1 Wing Weight Estimation Model

For the purpose of shifting wing weight estimation from the empirical methods of PACELAB APD 3.1 over to a more physics-based approach based on work accomplished in VT MDO, a new FEM-based model was implemented in PACELAB-VT by Dr. Davide Locatelli for more accurately calculating wing weight³⁸. This model also allows for including the influence of a strut on the wing model. The beam idealization of the wing-strut model assumes hinge points at the strut-wing, strut-fuselage and wing-fuselage intersections. Because of the presence of non-lifting struts, the strut only acts in tension and compression, and the impact of the strut on wing loading is a straightforward calculation.

The method calculates the wing material weight required to withstand the loads from eighteen load cases (see Table 22) based on wing geometry, fuel volume, engine and aerodynamic loads. The wing structure is a simple box shape and all the fuel onboard the airplane is assumed to be present within this wing box. Equations for secondary wing weights are taken directly from FLOPS².

Table 22. Load cases for wing sizing³⁸

Load Case Number	Load Case Type	Load Factor	Weight Configuration
1	Ultimate Load	+2.5	Max Payload (100% Fuel)
2	Ultimate Load	+2.5	Max Payload (50% Fuel)
3	Ultimate Load	-1	Max Payload (100% Fuel)
4	Ultimate Load	-1	Max Payload (50% Fuel)
5	Landing Loads	+3.5	MLW (100% Fuel)

6	Taxi Bump	+2	MRW (100% Fuel)
7	Gust, Approach	NA	MRW (100% Fuel)
8	Gust, Approach	NA	No Payload (0% Fuel)
9	Gust, Sea Level	NA	MRW (100% Fuel)
10	Gust, Sea Level	NA	No Payload (0% Fuel)
11	Gust, 10000 ft	NA	MRW (100% Fuel)
12	Gust, 10000 ft	NA	No Payload (0% Fuel)
13	Gust, 20000 ft	NA	MRW (100% Fuel)
14	Gust, 20000 ft	NA	No Payload (0% Fuel)
15	Gust, 30000 ft	NA	MRW (100% Fuel)
16	Gust, 30000 ft	NA	No Payload (0% Fuel)
17	Gust, 40000 ft	NA	MRW (100% Fuel)
18	Gust, 40000 ft	NA	No Payload (0% Fuel)

As discussed in Section 2.1.3, the aerodynamic load across the wing is assumed elliptical, and fuel loads are calculated from a simple volume computation. Given the loads and wing geometry, a simple FEM model is then used to calculate the necessary amount of material to withstand critical bending, torsion and shear stresses. This model subdivides the wing box into sections (or panels) with stiffeners at each panel end. The user specifies the stiffener cross-sectional area, the panel ‘width’ which is the distance between stiffeners along the wing box cross-section, and the panel ‘length’ which is the approximate distance between ribs. Figure 38 shows a single panel on top of the wing box. In the figure, there are ten panels total for the number of stiffeners present. The method then computes the required amount of material in each panel for the load cases and types (shear, torsion and bending).

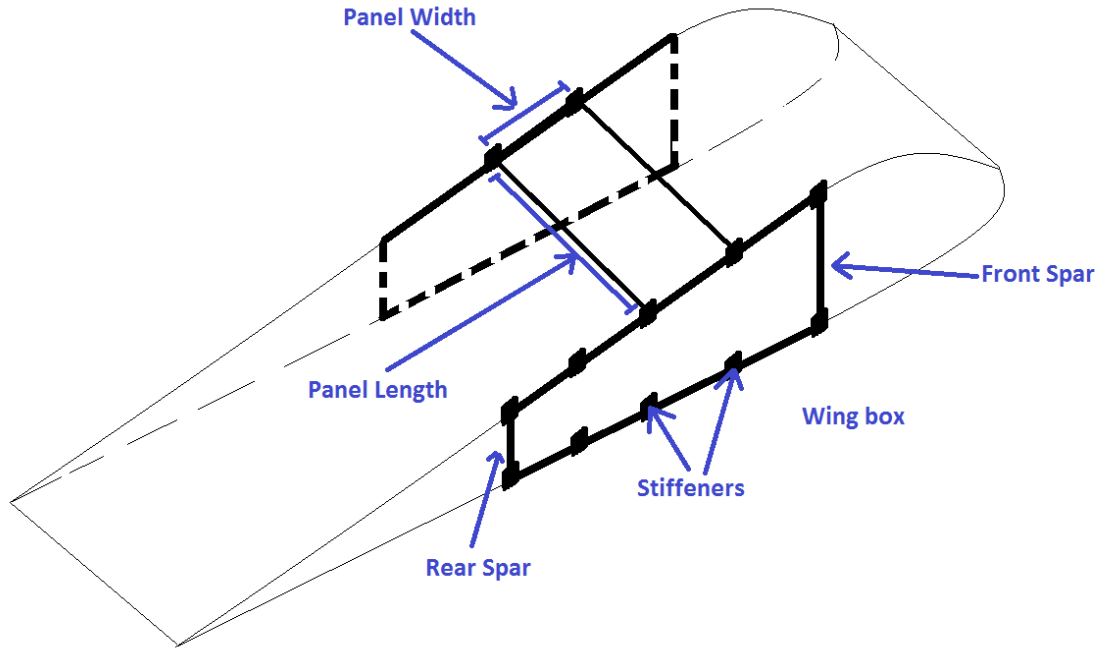


Figure 38. Wing box model

Validation results for the model can be seen in Figure 39 for the PACELAB-VT Boeing 777 aircraft. Next to critical bending stiffness, VT MDO calculated bending stiffness is plotted along with that calculated with the new method added to PACELAB-VT. If calculated bending stiffness dips below critical bending stiffness, the wing cannot sustain the loads on it. VT MDO structural calculation approximates the wing as two flat plates (no stiffeners), which tends to over-design the wing at the root and under-design it nearer to the tip. The PACELAB-VT method shows good agreement with the critical bending stiffness, however.

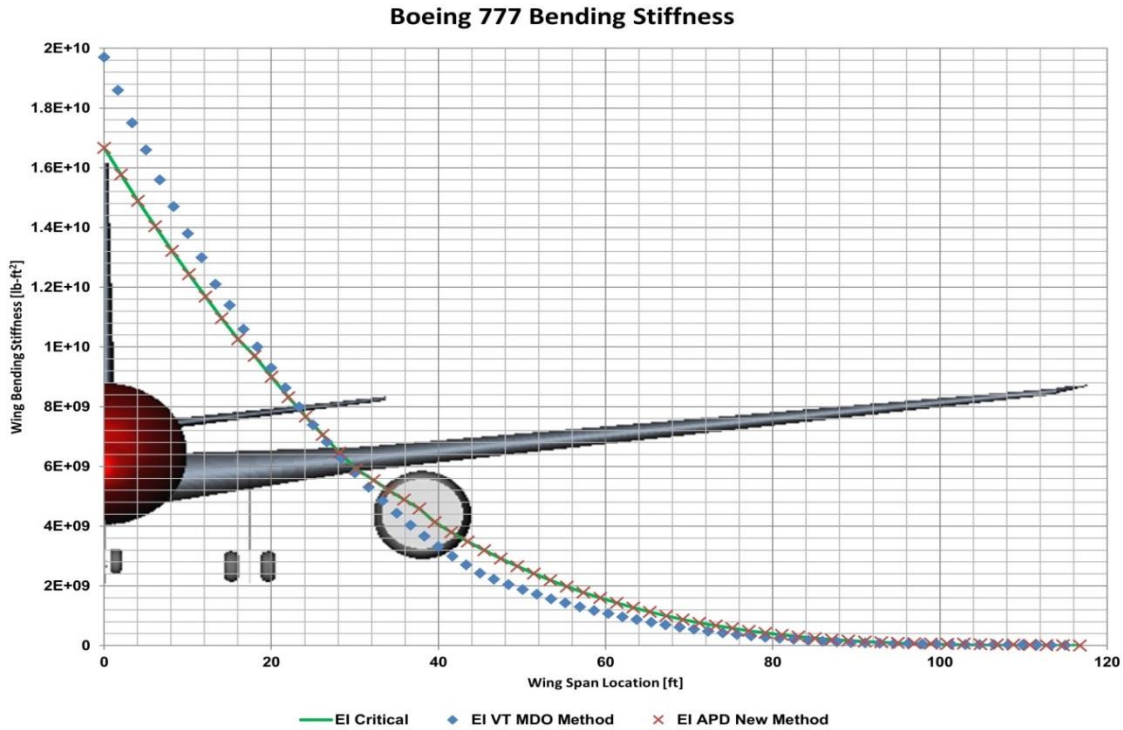


Figure 39. Bending stiffness validation for new PACELAB method²⁷

For further comparison, the new PACELAB-VT method was compared to other models for two aircraft, the 737-800 used in this study and a 777 model (taken from VT MDO), which is a much larger and heavier aircraft than the 737-800. The results show significant variance in the predicted wing weight (see Table 23).

Table 23. Wing weight predictions for both a 737-800 and 777 size aircraft

	Wing Weight 737 (lbs)	Wing Weight 777 (lbs)
VT MDO	16571	75757
PACELAB VT	13570	59692
PACELAB APD 3.1	14513	80145
Raymer	12610	70971
Nicolai	10093	52698
FLOPS	18967	70714

The original VT MDO wing weight method agrees well with historical data correlations by Shevell³⁹, however the reduced weight predicted by the new method in PACELAB is further from the curve. Figure 40 shows the wing weight of the 737 baseline aircraft (recall Section 1.5) as predicted by the original VT MDO method, and that predicted by the new method in PACELAB, plotted against Shevell’s wing weight curve, along with corresponding estimates from the other empirical and semi-empirical models (Torenbeek⁶, Raymer¹, Nicolai⁴⁰, and FLOPS²), seen in Table 23. The new PACELAB-VT model falls between the outliers seen in the left-hand side of Figure 40, but the differences among the models are significant.

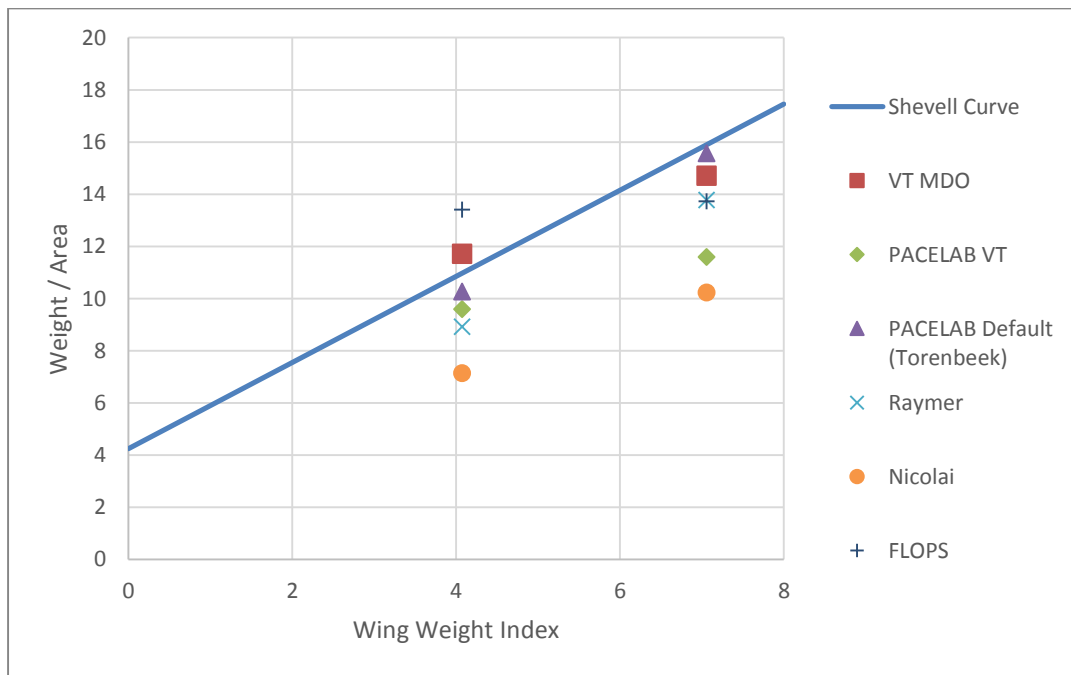


Figure 40. Shevell's wing weight curve with predictions from VT MDO, PACELAB APD 3.1 (Torenbeek), PACELAB-VT (Locatelli), Raymer and Nicolai. 737-800 on the left, 777 on the right.

Here, wing weight index is calculated from Equation 14, where N_{ULF} is the ultimate load factor (3.75), b is the wingspan, $TOGW$ is the takeoff gross weight, ZFW is

the zero fuel weight, λ is the wing taper ratio, $\frac{t}{c_{avg}}$ is the wing thickness ratio weighted average, Λ is the wing elastic axis sweep, and S_w is the wing area.

$$WWI = \frac{N_{ULF} b^3 \sqrt{TOGW \cdot ZFW} (1+2\lambda)}{\frac{t}{c_{avg}} \cos^2 \Lambda S_w^2 (1+\lambda)} \times 10^{-6} \text{ lb/ft} \quad \text{Eqn. 14}$$

While the lower predicted weight of the new method falls well below Shevell's curve, it does fall closer to other empirical correlations to data from Raymer¹ (Equation 15.25), Torenbeek⁶ and Nicolai⁴⁰ (Equation 20.2). A larger aircraft case (777-200ER) was also considered and plotted in Figure 40. Note that while the Raymer prediction diverges from PACELAB-VT with this heavier aircraft the Nicolai prediction is close to it. It is apparent that, depending on the source material, prediction for wing weight for any given aircraft can vary significantly. The differences in Figure 40 translate to a few thousand pounds worth of difference in actual wing weight for a 737-size aircraft (Table 23). Considering the TOGW of this aircraft is around 170000 pounds the relative differences in wing weight prediction are a small contribution to the overall aircraft weight. In the case of the aircraft in this study, which fall in the same class as the 737-800, the results from PACELAB-VT lie in the middle of the spread of possible values predicted by the other models.

2.3.2 Engine Scaling Model

A simple 'rubber-engine' model from the VT MDO code, based on work by Mattingly⁴¹, was also implemented in PACELAB-VT that scales the engine weights and dimensions with maximum thrust available and a reference engine (in this case the CFM-56B24 for the nominal 737-800 mission). Equations 15-17 show the relationship between

thrust and the weight / dimensions of the engines, and Table 24 contains the referenced values utilized in this study.

$$L_{nacelle} = L_{ref} \sqrt{\frac{T_{max}}{T_{ref}}} \quad \text{Eqn. 15}$$

$$D_{nacelle} = D_{ref} \sqrt{\frac{T_{max}}{T_{ref}}} \quad \text{Eqn. 16}$$

$$W_{eng} = W_{ref} \frac{T_{max}}{T_{ref}} \quad \text{Eqn. 17}$$

Table 24. Engine reference values¹⁴

Dry engine mass (lbs)	5216
Nacelle length (ft)	10.14
Nacelle width (ft)	6.76

Because of the simplicity of this model, validation consisted only of looking at the output values for engine weight and dimensions, and verifying they matched to the appropriate input value for maximum thrust.

CHAPTER 3: Aircraft Design Studies

In this chapter are presented the minimum-fuel optimization results for two configuration types: cantilever and strut-braced wing aircraft. The mission as discussed in Section 1.5 is representative of a mid-range regional airliner, and the baseline aircraft for starting the optimization runs is identical to the 737-800 presented in Section 2.1.5.2 for the aerodynamic method validation.

Comparisons are also shown for these optimizations in different software and using different options. For the cantilever aircraft, results are shown from VT MDO, PACELAB APD 3.1 methods, the new methods in PACELAB-VT as presented in this study, and FLOPS. For the SBW aircraft, only VT MDO and new PACELAB-VT results are shown, as FLOPS does not fully model the SBW configuration, and, of course, PACELAB APD 3.1 methods are inadequate.

3.1 Cantilever Aircraft Designs

Design variables for this configuration are discussed in Section 1.4.2. These optimizations were performed in PACELAB-VT and PACELAB APD 3.1 using an approach similar to that used in similar runs in past VT MDO studies¹⁴, where a global-search method (Frontline Evolutionary) generates initial conditions for a gradient-based solver (CONMIN), thus approaching a global minimum.

Figure 41 and the first two columns of Table 25 show results for the minimum-fuel optimized cantilever aircraft in PACELAB APD 3.1 and PACELAB-VT (left and right, respectively). Reduction in fuel load from the baseline case of 45300 lbs is predicted to be 10% with the PACELAB APD 3.1 methods, and fuel savings are

estimated at 23% with the new methods in PACELAB-VT. The lower fuel savings with PACELAB APD 3.1 is due to the higher drag and aircraft weight estimation.

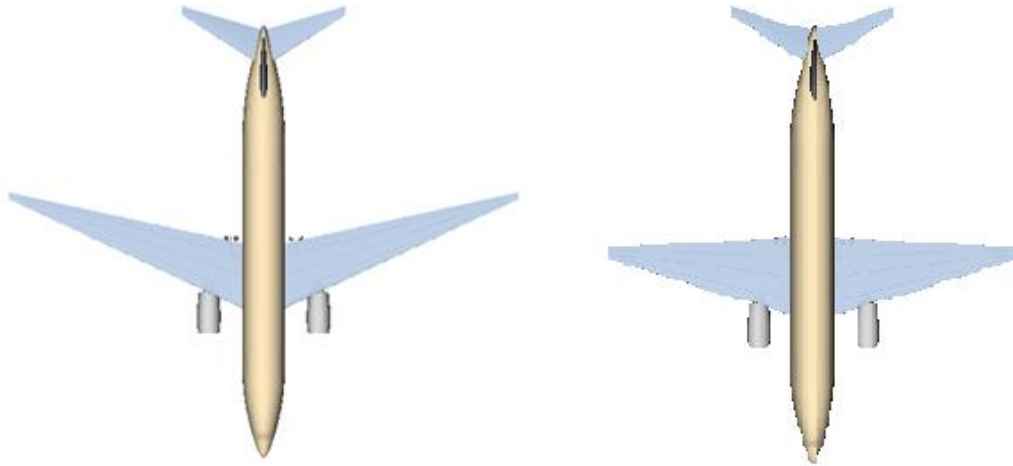


Figure 41. Optimized cantilever aircraft in PACELAB APD 3.1 (left) and PACELAB-VT(right)

The most obvious visual difference between the two aircraft is the decrease in wing sweep with the new methods and the shorter wingspan. This is due to the reduction in drag predicted by the VT MDO aerodynamic methods compared to PACELAB APD 3.1 (see Section 2.1.5.2). Reduction in wing thickness also decreases the wave drag compared to the PACELAB APD 3.1 case (see Table 25). Importantly, because the PACELAB APD 3.1 methods do not calculate moment along the span, the tip deflection constraint could not be enforced for that aircraft, thus the wingspan was allowed to be higher for the final configuration. A lower TOGW (due to the wing weight reduction) also could explain the decrease in wingspan (and thus wing area), as a smaller wing is needed for carrying the same payload, and less space is needed for fuel. As discussed

earlier, wing weight predictions from VT MDO are high compared to those in the new PACELAB-VT weight method, resulting in a much higher predicted wing weight. The effect of the increased wing weight in the VT MDO predictions results in a larger wing, which also results in the higher lift-to-drag ratio and TOGW than that of the PACELAB-VT methods. Due to the presence of more wing material, tip deflection is decreased thus allowing the wingspan to be longer.

Table 25. Optimized minimum fuel cantilever aircraft

Parameter	PL APD	PL VT	VT MDO	FLOPS
Fuel Weight (lbs)	40810	34839	31300	41720
Wing Weight (lbs)	25948	14337	34100	17468
TOGW (lbs)	185800	163000	168200	170061
Cruise L / D	22.07	23.1	31.1	17.7
Wing Area (ft ²)	1640	1653	2260	1580
Cruise Altitude (ft)	38116	38700	42900	35216
Maximum Thrust (lbf)	23375	20608	19200	24572
Wing Root Chord (ft)	18.93	22.43	24.79	22.86
Wing Tip Chord (ft)	2	3.65	2.23	2.29
Wing Quarter Chord Sweep (deg)	22.06	12.47	0	16.67
Wing Span (ft)	147.2	118.5	167	125.7
Wing Root Thickness Ratio	0.011	0.066	0.064	0.092
Wing Tip Thickness Ratio	0.05	0.086	0.06	0.092

The optimized aircraft from VT MDO and FLOPS are shown in Figure 42 and the third and fourth columns of Table 25. VT MDO predicts a fuel savings of 32% from the baseline aircraft fuel load, while FLOPS predicts a small increase in savings. Recall that the optimization methods available in FLOPS are gradient-based solvers that do not necessarily approach a global minimum, thus the FLOPS results are dependent on the initial starting conditions for the design variables.

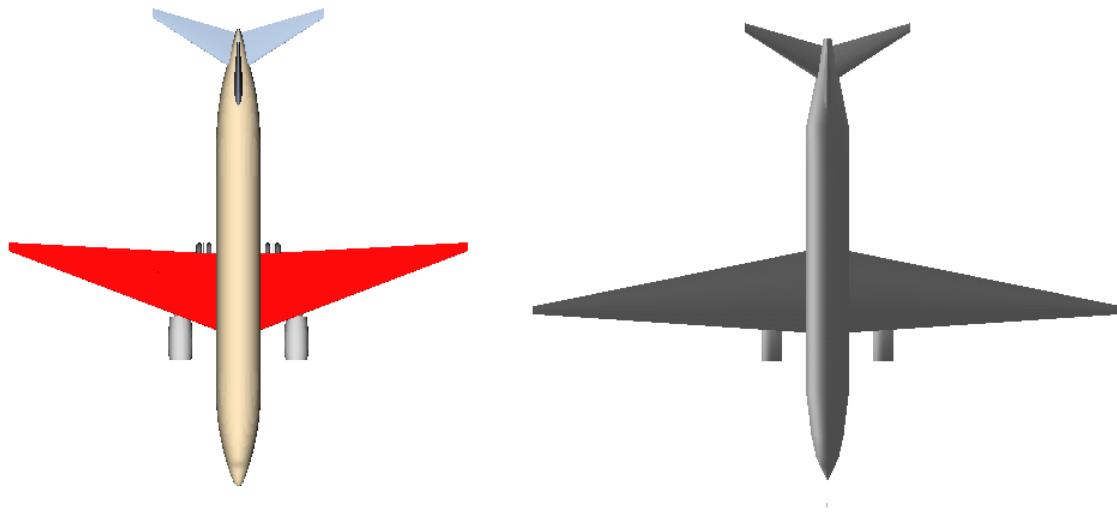


Figure 42. Optimized cantilever aircraft from FLOPS (left) and VT MDO (right)

An interesting point of note in the FLOPS results is the lower predicted cruise lift-to-drag ratio. The FLOPS aerodynamic calculation is based on decades-old empirical methods⁴², and it predicts a transonic drag rise much sooner than the other, newer models. Therefore, it is expected that an aircraft flying in the transonic regime would have an estimated drag penalty much higher in FLOPS. A comparison study⁴³ conducted between PACELAB APD 3.1 and FLOPS for a similar aircraft (737-800, analysis only) showed FLOPS predicts a higher wave drag penalty due to an earlier drag rise (see Figure 43). Friction drag estimates in FLOPS are also significantly higher (on the order of 40 drag counts) at cruise conditions. The result of this is a decreased lift-to-drag ratio, and the necessity for more fuel and a more powerful engine.

For the similarly-sized wings of the PACELAB-VT aircraft and that calculated by FLOPS, estimated wing weights are within 20% of each other. Predictions from Torenbeek and VT MDO are significantly higher due to increases in wing size and the difference in the weight estimation models, as discussed in Section 2.3.1.

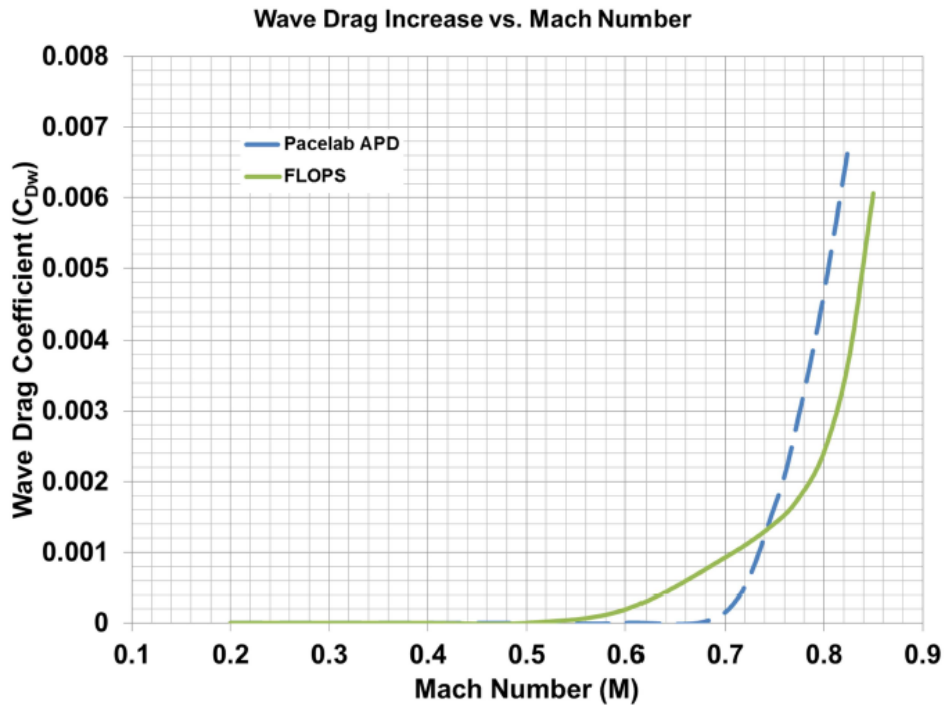


Figure 43. Wave drag rise for 737-800 model in default PACELAB and FLOPS⁴⁰

3.2 Strut-Braced Wing Aircraft Designs

Other than the addition of new design variables as shown in Tables 1 and 2, optimization, mission and constraint settings for the strut-braced wing optimization are identical to those for the cantilever aircraft. Recall the assumption of a constant chord, constant thickness ratio strut. While the model implemented in PACELAB-VT does allow for varying thickness ratios and chord for the strut by defining those properties at the centerline and strut tip cross sections separately, for this study they were kept constant to reduce the complexity of the model.

The left-hand side of Figure 44 and the first column in Table 26 show the minimum-fuel optimized strut-braced wing aircraft (non-lifting struts) from the new

PACELAB-VT framework. The optimized aircraft predicts fuel savings of 37% compared to the baseline 737 fuel load of 45300 lbs.

The design produced by the VT MDO code is shown on the right-hand side of Figure 44 and in the second column of Table 26. VT MDO fuel reduction with its own optimized aircraft is about 28% compared to the baseline.

The two aircraft are visually similar with the most notable differences being the longer chord near the wing root of the PACELAB-VT model, as well as a small increase in wing sweep. The PACELAB-VT aircraft has higher fuel savings, as well as a higher lift-to-drag ratio in cruise configuration. Wing weight estimations between the two models are significantly different, as is expected (recall the discussion in Section 2.3.1). Interestingly, it was found that during experimentation with the VT MDO model (which uses the Trefftz analysis approach for the induced drag, optimizing the spanloads for minimum induced drag), allowing lift to be present on the strut actually dramatically improves performance, increasing the cruise lift-to-drag ratio to 31.7, and reducing the required fuel load to 28600 lbs, an increase of 9% in fuel savings over the non-lifting case.

Finally, the longer span of the PACELAB-VT aircraft results in a higher wing area, and combined with the lower wing weight, this results in the PACELAB-VT aircraft having lower wing loading than its VT MDO counterpart, which is an indicator of higher maneuverability and better takeoff and landing performance.

Table 266. Optimized minimum fuel SBW aircraft

Parameter	PL New	VT MDO
Fuel Weight (lbs)	29250	33140
Wing Weight (lbs)	23029	30800
TOGW (lbs)	166974	170388
Cruise L / D	30.3	27.5

Wing Area (ft ²)	1935	1583
Cruise Altitude (ft)	43700	40200
Maximum Thrust (lbf)	22019	26500
Wing Root Chord (ft)	13.71	8.79
Wing Kink Chord (ft)	11.13	11.89
Wing Tip Chord (ft)	3.892	3.85
Wing Quarter Chord Sweep (deg)	16.7	13.8
Strut / Wing Half-Span (ft)	51.9 / 94.1	41.7 / 87.4
Wing Root Thickness Ratio	0.09054	0.05799
Wing Kink Thickness Ratio	0.07188	0.07076
Wing Tip Thickness Ratio	0.08712	0.05152
Strut Chord (ft)	7.012	12.2
Strut Thickness Ratio	0.09216	0.06408

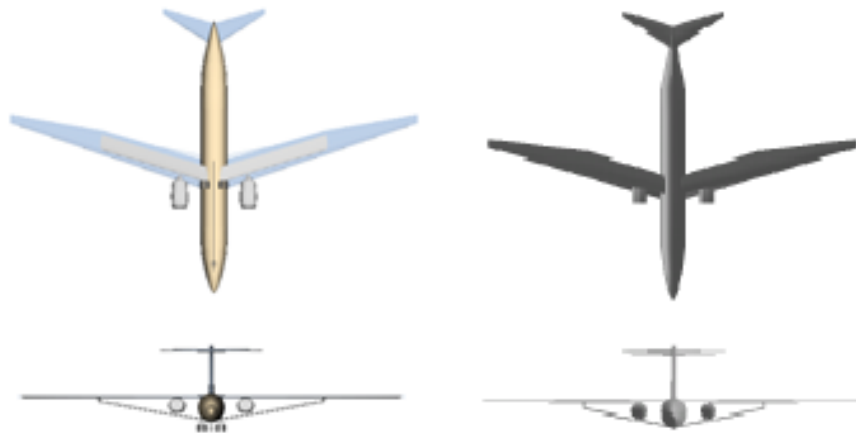


Figure 44. PACELAB optimized SBW (left) and VT MDO optimized SBW (right)

While the fuel savings with this configuration are very high compared to the baseline cantilever aircraft, strut-braced wing aircraft might incur costs in airport space due to the higher wingspan (the airport limit is about 80 meters, or 250 feet). Thus, in many configurations in VT MDO it is assumed that there is within the wing (usually at the strut intersection point) a wing-fold mechanism that is represented in the model by a weight penalty within the wing. For this initial framework development in PACELAB-VT, this was not considered, but would be an issue that could be studied in future work.

CHAPTER 4: Conclusions

Over the course of this study, new methods were implemented for expanding the capability of PACELAB APD 3.1 to handle new aircraft configurations, as well as improve the accuracy of the calculations by replacing or augmenting existing empirical methods with physics-based methods based on work done at Virginia Tech.

A new aerodynamic model was implemented in PACELAB-VT which allows the user more control and provides more complex, physics-based models for the calculation of characteristics such as transition and interference drag effects, implementation of airfoil shape effects in wave drag estimation, and the estimation of strut aerodynamics as well. Detailed validation and quantification of differences from existing VT MDO aerodynamics calculations and those newly implemented in PACELAB-VT were carried out. A simple ‘rubber-engine’ size / weight scaling calculation was added to PACELAB-VT, as well as a new method for wing weight estimation used to evaluate the effect of the strut, as well as more accurately model the wing than the prior default empirical methods.

Minimum fuel optimizations were performed in PACELAB-VT with both these new methods and existing default methods (where they could be applied), and results were compared with similar optimizations in VT MDO and FLOPS, two veteran MDO applications. Fuel savings of 37% were predicted in PACELAB-VT and of 28% in VT MDO for a strut-braced wing aircraft, while savings ranging from 10-30% for an optimized cantilever aircraft were found. FLOPS and PACELAB APD found fuel savings of 9% and 10%, respectively, for the cantilever aircraft, due to the higher drag estimations from their aerodynamic methods. Aside from these results, it was also demonstrated that PACELAB APD has potential for future MDO applications, based on

its flexible optimization scheme and mixture of both global-search and local gradient-based solvers for use in the optimization process, similar to the framework in place within VT MDO.

Work has already begun on adding a new, generalized induced drag method based on a Trefftz plane analysis approach⁴⁴ to a newer version of PACELAB APD (3.5). This new version allows for more flexibility in defining wing shapes (multiple trapezoidal shapes, no fixed leading edge), and adding this Trefftz method for induced drag would allow the induced drag contribution to be estimated for any planar, lift-carrying surface present on the vehicle, including struts. Because the Trefftz analysis also gives the lift distribution on lift-carrying surfaces, the wing weight and aerodynamic methods can then be linked, so the aerodynamic module calculates the load distribution across the wing and the wing weight module then uses that distribution to appropriately size the wing.

PACELAB-VT is also currently being adapted to handle other nonconventional aircraft configurations such as tailless and hybrid wing-body aircraft. While the methods implemented in this study (and the induced drag method to be finished in the near future) would be enough to handle these configurations, other portions of the PACELAB-VT model, and the underlying software source code, would not recognize these types of aircraft and would generate errors. Thus, a significant expansion / reworking of the PACELAB-VT code is anticipated.

Other possibilities for future work could be further enhancement of the aerodynamic model through CFD or experimental results, allowing the user to add juries to the strut (to make a truss-braced wing), improving calculations for stability and control, extension of the wing weight method to the empennage, and others.

References

- ¹ Raymer, D., “Aircraft Design: A Conceptual Approach. 5th ed.”, (AIAA Education Series. Reston, VA: American Institute of Aeronautics and Astronautics, 2012), ISBN-10: 1600869114.
- ² McCullers, L.A. “FLOPS: Aircraft Configuration Optimization”, NASA CP-2327, 1984.
- ³ Ashley, H. “On Making Things the Best – Aeronautical Uses of Optimization”, AIAA Journal of Aircraft Vol. 19, No. 1. 1984, doi: 10.2514/3.57350.
- ⁴ Grasmeyer, J. M. “Multidisciplinary Design Optimization of a Strut-Braced Wing Aircraft”, Master’s Thesis, Virginia Tech, 1998.
- ⁵ Gur, O., Bhatia, M., Mason, W., Schetz, J. et al., “Development of a framework for truss-braced wing conceptual MDO”, presented at the 6th AIAA Multidisciplinary Optimization Specialist Conference, USA, April 12-15, 2010, doi: 10.1007/s00158-010-0612-9.
- ⁶ Torenbeek, E., “Synthesis of Subsonic Airplane Design”, (Delft: Delft University Press, 1984), ISBN-10: 9024727243.
- ⁷ Boone, T. R. and Striz, A. G. “Optimization of Aircraft Configuration for Minimum Drag”, presented at the 51st AIAA/ASME/ASCE/AHS/ASC Structures, Structural Dynamics and Materials Conference, USA, 12-15th April 2010, doi: 10.2514/6.2010-3000.
- ⁸ Gur, O., Mason, W., Schetz, J., “Full Configuration Drag Estimation”, presented at the 27th AIAA Applied Aerodynamics Conference, USA, 22-25 June 2009, doi:10.2514/1.47557.
- ⁹ McDonald, M., “The Effect of Reducing Cruise Altitude on the Topology and Emissions of a Commercial Transport Aircraft”, M.S. Thesis, Virginia Tech, 2010.
- ¹⁰ Peoples, Willcox, “Value-Based Multidisciplinary Optimization for Commercial Aircraft Design and Business Risk Assessment”, Journal of Aircraft Vol. 43, No. 4 July-Aug 2006, pp. 913-921, doi: 10.2514/1.14147.
- ¹¹ Choi, S., “Multi-Fidelity and Multi-Disciplinary Design Optimization of Supersonic Business Jets”, PhD. Dissertation, Stanford University, 2005.
- ¹² Vanderplaats, G. N. “Automated Optimization Techniques for Aircraft Synthesis”, AIAA Paper 76-909, 1976.

¹³ Web. <http://www.transtats.bts.gov/fuel.asp>. US Department of Transportation, Bureau of Transportation Statistics. Accessed 1/2015.

¹⁴ Meadows, N., “Multidisciplinary Design Optimization of a Medium Range Transonic Truss-Braced Wing Transport Aircraft”, M.S. Thesis, Virginia Tech, 2011.

¹⁵ Ting, E., Reynolds, K., Nguyen N., Totah, J., “Aerodynamic Analysis of the Truss-Braced Wing Aircraft Using Vortex-Lattice Superposition Approach”, presented at the 32nd AIAA Applied Aerodynamics Conference, 2014, doi: 10.2514/6.2014-2597.

¹⁶ Gundlach, J., Tetrault, P., Gern, F., Nagshineh-Pour, A., et al “Conceptual Design Studies of a Strut-Braced Wing Transonic Transport”, *Journal of Aircraft* Vol. 37, No. 6, Nov-Dec 2000, pp. 976-983, doi: 10.2514/2.2724.

¹⁷ Grasmeyer, J.M., et al. “Multidisciplinary Design Optimization of a Strut-Braced Wing Aircraft with Tip-Mounted Engines.” MAD Center Report 98-01-01, Virginia Tech, 1998.

¹⁸ Gur, O., Bhatia, M., Schetz, J.A., Mason, W.H., et al., “Multidisciplinary design optimization of truss braced wing aircraft”, AIAA Paper 2009-7114, presented at the 9th AIAA Aviation Technology, Integration, and Operations Conference and Aircraft Noise and Emissions Reduction Symposium, September 21-23, 2009, Hilton Head, South Carolina.

¹⁹ Leifsson LT (2005) Multidisciplinary design optimization of low-noise transport aircraft. Ph.D. thesis, Virginia Polytechnic institute and State University.

²⁰ Wells, D., Olson, E., “Hybrid Wing Body Planform Design with Vehicle Sketch Pad”, presented at the 49th AIAA Aerospace Sciences Meeting Including the New Horizons Forum and Aerospace Exposition, Jan 4-7 2011, Orlando, Florida.

²¹ PACE GmbH, “PACELAB APD 3.1 User Documentation”, PACELAB User Documentation, 2013.

²² Gur et al. “Truss-Braced Wing MDO in ModelCenter Framework.” MAD Center Report 2010-01. 2010.

²³ Gur, O., Schetz, J., Mason, W., “Aerodynamic Considerations in the Design of Truss Braced Aircraft”, presented at the 28th AIAA Applied Aerodynamics Conference, USA, 28 June 2010, doi: 10.2514/1.C031171.

²⁴ ModelCenter 9.0 Manual. Phoenix Integration, 2011.

²⁵ Tétrault, P.-A., Schetz, J. A., Grossman, B., “Numerical prediction of the interference drag of a strut-surface intersection in transonic flow,” *AIAA Journal*, Vol. 39, No. 5, May 2001, pp. 857-864.

²⁶ Anderson, J. A. “Fundamentals of Aerodynamics 5th ed”, (AIAA Aviation Series, 2010), ISBN-10: 0073398101.

²⁷ Braslow, A. L., Bartlett, D. W., Wagner, R. D., and Collier Jr., F. S., “Applied Aspects of Laminar-Flow Technology,” *Viscous Drag Reduction in Turbulent Boundary Layers*, edited by D. M. Bushnell and J. N. Hefner, *Progress in Aeronautics and Astronautics*, AIAA, New York, 1990.

²⁸ White, F.M., “Viscous Fluid Flow”, (McGraw-Hill New York, 1974), pp. 589-590, ISBN-10: 0072402318.

²⁹ E.J. Hopkins and M. Inouye, “An Evaluation of Theories for Predicting Turbulent Skin Friction and Heat Transfer on Flat Plates at Supersonic and Hypersonic Mach Numbers,” *AIAA J.*, Vol. 9, No. 6, June 1971, pp. 993-1003.

³⁰ Hopkins, E.J., “Charts for Predicting Turbulent Skin Friction From the Van Driest Method (II),” *NASA TN D-6945*, October 1972.

³¹ Cebeci, T., and Bradshaw, P., “Momentum Transfer in Boundary Layers”, (McGraw-Hill New York, 1977), pp. 187.

³² Jobe, C.E., “Prediction and verification of aerodynamic drag, part I: prediction”, Chapter IV in *Thrust and Drag: Its Prediction and Verification*, Ed. Eugene, C.E., Vol. 98 *Progress in Astronautics and Aeronautics*, AIAA, Broadway New York, 1985.

³³ Inger, G.R., “Application of Oswatitsch’s theorem to supercritical airfoil drag calculation,” *Journal of Aircraft*, Vol. 30, No. 3, May-June 1993, pp. 415-416.

³⁴ Hilton, H.W., “High speed Aerodynamics”, (Longmans, Green and Co., London, 1951), ISBN-10: 1124045724.

³⁵ Mason W., “Analytic models for technology integration in aircraft design”, AIAA 90-3263, presented at *AIAA/AHS/ASEE Aircraft Design, Systems and Operations Conference*, USA, September 17-19, 1990.

³⁶ PACE GmbH, “Calculation Methods Reference PACELAB APD 3.1”, *PACELAB User Documentation*, 2013.

³⁷ Hoerner, S. F., “Fluid Dynamic Drag”, (Hoerner Fluid Dynamics, Bakersfield, CA, 1965), ISBN-10: 9993623938.

-
- ³⁸ Locatelli, D., “WP3 Wing Weight Estimation Method”, VT report presented to SNECMA, 2014.
- ³⁹ Shevell, R. S., “Fundamentals of Flight 2nd Ed.”, (Prentice Hall, 1988), ISBN-10: 0133390608.
- ⁴⁰ Nicolai, L. M., “Fundamentals of Aircraft and Airship Design”, (AIAA, 2011), ISBN-10: 1600867510.
- ⁴¹ Mattingly, J. “Elements of Gas Turbine Propulsion”, (McGraw-Hill, 1996), ISBN-10: 0071145214.
- ⁴² Feagin, Richard C. and Morrison, William D., Jr.: Delta Method, An Empirical Drag Buildup Technique. NASA CR-151971, December 1978.
- ⁴³ Locatelli, D., Riggins, B., Schetz, J.A., Kapania, R.K., et al., “Aircraft Conceptual Design: Tools Evaluation”, presented at the 14th AIAA Aviation Technology, Integration, and Operations Conference, June 16-20 2014, Atlanta, Georgia, doi: 10.2514/6.2014-2030.
- ⁴⁴ Grasmeyer, J.M., “A Discrete Vortex Method for Calculating the Minimum Induced Drag and Optimum Load Distribution for Aircraft Configurations with Non-coplanar Surfaces,” VPI-AOE-242, January, 1997.